Abstract

Micro-Electro-Opto-Mechanical-Systems or MOEMS have potential applications *inter alia* in biomedical research. For instance, studies of the Bystander Effect require controlled irradiation of biological cells with focused X-rays to reveal the mechanisms occurring.

X-ray focusing may be achieved using an adaptive optic micro-lens in which focusing is entirely reflective and therefore compatible with broad band illumination, an improvement over diffractive systems such as zone plates. Such a micro-lens can be microfabricated in the form of a bent-cantilever beam made from two dissimilar materials (polyimide and gold) in a thermal bimorph configuration, actuated with a micro heater. The parallel horizontal slots on the beam provide the transmission and focusing functions, while the heater provides control of the focal length through variation of the beam's curvature. This novel system has been named 1D-MOXI (Micro-Opto-X-ray Imaging) and a basic system has already been made and tested thermo-mechanically.

The present work focuses on details of the geometry of the deformed slotted micro-beam lens element under thermally derived strain, using finite element analysis, and suggests an optimized MOEMS design, giving prescribed curvature of the lens through changing the number and the dimensions of the slots.

The study reveals the localized stress and the small deviations of the micro-lens behavior from that of perfect spherical geometry. The focal length variation with temperature is compared with the experimental values and those predicted by an analytical model.

Summary

1. Glossary

There are several words which are used frequently in this thesis as bellow:

MOEMS: Micro-Opto-Electro-Mechanical System.

FEA: Finite Element Analysis.

Microcantilever: Cantilever in micron size.

Microchannel: Channel in micron size.

2. Preface

2.1. Origin of the Project

This project is done to improve a novel MOEMS mechanism employed for Xray focusing. The application of Xray focusing in this project is the application named *"inter alia"* in biomedical research.

2.2. Motivation

As an example, studies of the Bystander Effect in biomedical researches require controlled irradiation of biological cells with focused X-rays to reveal the mechanisms occurring. This application led us to concentrate on the modeling and optimization a microcantilever used in the Xray imaging lens.

2.3. Project Requirements

We used ANSYS -Release 9- software for the Finite Element Analysis.

2.4. Outline

This Report is organized as follow: Section 3 describes the Xray focusing history and the one dimensional Micro-Opto-Xray Imaging Lens. Theoretical modeling of flat and bent microcantilever is compared with finite element analysis. The FE analysis includes thermal analysis and thermal-structural analyses -both linear and non-linear- of the microlens represented in section 4 and are compared with experimental results. Section 5 suggests an optimized MOEMS design using finite element analysis. Finally, results and conclusion sections conclude this work.

3. Introduction

Micro electro Mechanical System is a multidisciplinary field in science. One of its subdivisions is Micro-Opto-Electro-Mechanical System having optoelectronic functional elements. Many applications require scanning, switching, deflecting, reflecting and focusing of an optical beam. Particularly, Focused X-Rays are of interest to study the so-called Bystander Effect, in which cells other than those irradiated are affected by the X-ray does [1, 2]. This requires focusing to a spot diameter on the micron scale. The system is an integration of a flexible micro-lens, sensor and mechanical actuation mechanism with an electromechanical control system to set the require focal length. The design and microfabrication of a one dimensional focusing MOEMS (1-D MOXI) system for use *"inter alia"* in X-ray analysis of biological cells was reported in [3].Two dimensional MOXI based adaptive optics for X-ray focusing was suggested in [4].

3.1. Xray Focusing

Conventional optics for focusing X-rays have low optical efficiency and are wavelength dependent, using zone plates or multilayer mirrors [5, 6]. An alternative approach is grazing incidence reflective optics, which provides high efficiency, but suffers from aberration limitations. For example, a microchannel plate (MCP), originally intended for electron multiplication, can be curved and "slumped" to form a reflective polycapillary focusing element, which has been used successfully in Xray imaging applications such as astronomy. The plate is mechanically deformed to provide the curved surface required for focusing [6]. Even with the most advanced manufacturing techniques, MCP channel diameters are limited to a minimum of 0.5 μm, over a few tens of millimeters and can produce focused spot sizes no smaller than 10 μm. Performance is limited by channel tilting, incorrect curvatures, waviness, diffraction and uncontrolled and limited substrate bending [7].

Recently, a microfabricated optical array for X-ray imaging (MOXI) was suggested as an alternative [7, 8]. The MOXI approach has similar advantages to those of a polycapillary system, including large aperture, high photon flux, large bandpass $\Delta\lambda/\lambda$ and high transmission, due to the low losses at grazing incidence. The basic optical element is shown schematically in Fig. 3.1. Reflection takes place on the sidewalls of a series of microchannels with a combination of a curved and flat plate forming the MOEMS device (microlens). The 1-D MOXI shown in Fig. 3.2 provides focusing in one dimension; a spot can be achieved by using two such microlenses in the so-called Kirkpatrick-Baez configuration [9]. A series of microchannels, formed from concentric rings of an

absorber/reflector such as Ni or Au, is deformed by radial actuators which also support the ring structure. A combination of a curved element and a flat one, as shown in Fig. 3.1, forms the optical system. A prototype two dimensional focusing system using gold reflectors on a flexible membrane substrate has been developed, using variable vacuum pressure to produce a zoom focusing effect [10].

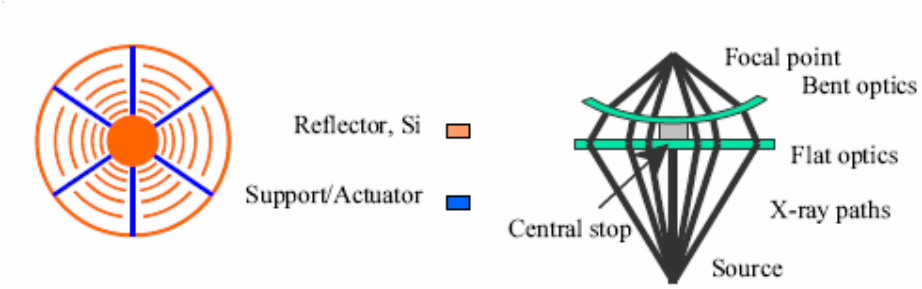

Fig._3.1._Schematic of the basic optical element a) - Multichannel MOXI reflective element with bimorph actuator/supports [6] b) - a pair of curved and flat optical elements are used for focusing.

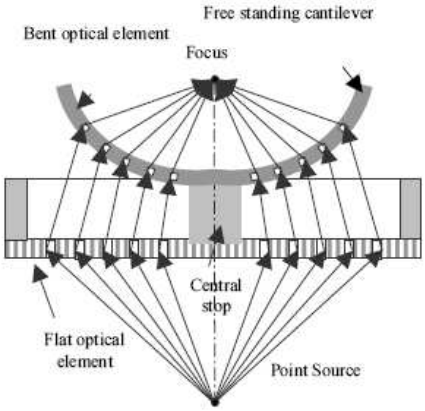

Fig._3.2._Schematic of 1-D MOXI system

3.2. Design of 1-D MOXI

The system consists of a micro-lens structure for focusing the X-rays, an actuation mechanism for changing the focal length and a micro-sensor for the feedback control system. The micro-lens consists of two optical elements, a lower flat element and an upper curved element; both are 8 μm thick with a width/space ratio of 5-7 μm. The bent optical element consists of two free-standing, out of plane cantilevers, anchored together through a central stop. The system is designed to reflect the X-rays at an angle less than the incident angle. The structures are etched through into the bulk substrate, to form a grating of microchannels.

The separation of the two optical elements by a distance of 3mm facilitates the range of movement of the bent optical element, giving a wide range of focal length through actuation. The actuation mechanism is controlled and activated by PC, with a feedback control system to define the required focal length. For this purpose a micro-sensor is integrated in the MOXI system to sense the curvature change of the cantilever.

The micro-sensor is a simple gold resistive strain gauge measuring small changes in deformation of the structure [11]. An early design was based upon a dry etched single crystal silicon wafer to form the optical elements, but this was superseded by the use of polyimide, which, when coated with a layer of gold, is readily formed into thermal bimorph cantilever actuators.

In the case of a free standing cantilever, the maximum strain is at the edge where the cantilever is anchored, so the sensing element is located there (Fig. 3.3).

The present work focuses on details of the geometry of the deformed slotted micro-beam lens element under thermally derived strain, using finite element analysis, and suggests an optimized MOEMS design, giving prescribed curvature of the lens through changing the number and the dimensions of the slots. The study reveals the localized stress and the small deviations of the micro-lens behavior from that of perfect spherical geometry. The focal length variation with temperature is compared with the experimental values and those predicted by an analytical model.

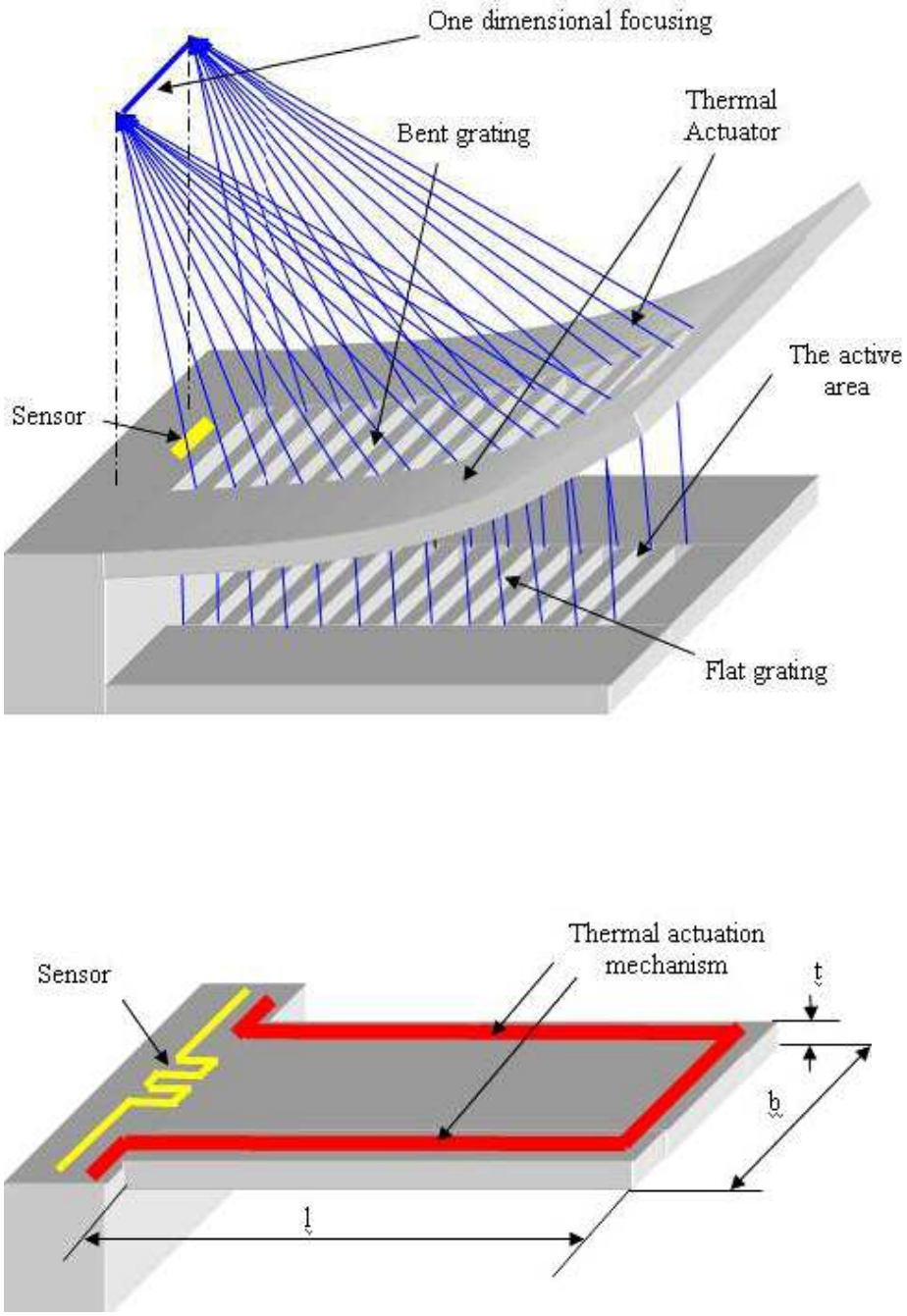

Fig._3.3._Design Concept of 1-D MOXI System

4. Theoretical Modeling and Analysis

This section provides the analytical and FEA solutions for a simple bimorph microcantilever, as described in the foregoing with and without the microchannels or slots.

4.1. Analytical Model

4.1.1. Flat Microcantilever Analytical Model

The bimorph actuator is a sandwich of two layers of dissimilar materials with an embedded metal micro-heater. Its operation relies upon the difference in linear thermal expansion between the two layers to produce large displacements perpendicular to the strain plane. In our design, the micro-heater is located at the outer boundary of the cantilever. Fig. 4.1 shows the simple model for deflection of the bimorph cantilever. The radius of curvature adopted when the structure is heated through a temperature change ΔT degrees is [11, 12]:

$$r = \frac{\frac{E_1 t_1^{\,3}}{E_2 t_2} + \frac{E_2 t_2^{\,3}}{E_1 t_1} + 6t_1 t_2 + 4t_1^{\,2} + 4t_2^{\,2}}{6(t_1 + t_2)(\alpha_2 - \alpha_1)\Delta T} \qquad \text{(Eq 4.1)}$$

Where E_i and t_i are the elastic modules and the layer thicknesses and α_i is the coefficient of linear expansion.

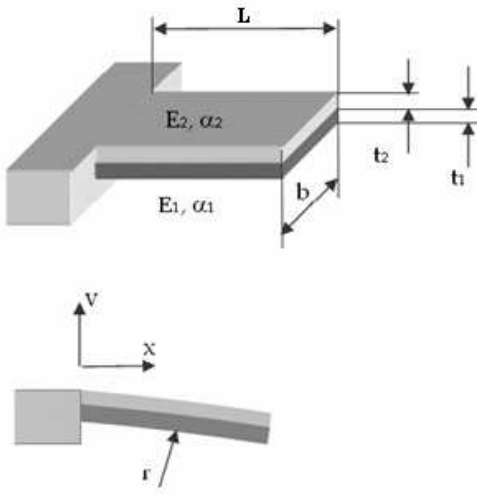

Fig._4.1._Model of bimorph cantilever deflection

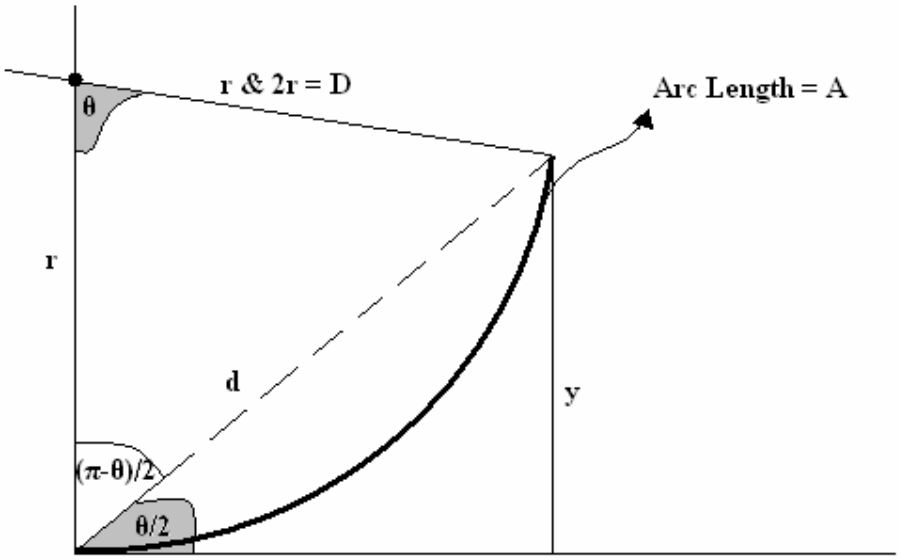

Fig._4.2._Geometric schematic of a bent beam.

The vertical displacement *y* of the end point of the cantilever can now be calculated from the radius of curvature as bellow and by using Fig. 4.2.

$\theta = A/r,\ d = 2r \sin(\theta/2)$ (Eq 4.2)

$y = 2r \sin^2(\theta/2)$ (Eq 4.3)

$y = 2r \sin^2(A/D)$ (Eq 4.4)

where *a* is the arc length and *D* the diameter of the circle of which the beam is a part.

The above analytical model does not take into account any effects due to the presence of the microchannels or slots in the beam. The comparison between the results obtained from analytical, finite element analysis and experiments will be discussed later, when we will see that the results of this simple model deviate substantially from the experimental values.

4.1.2. Bent Microcantilever Analytical Model

It will be helpful if one concerns a bent bimorph cantilever beam. Several problems have been solved about the bending for a uniform material bent beam [13].

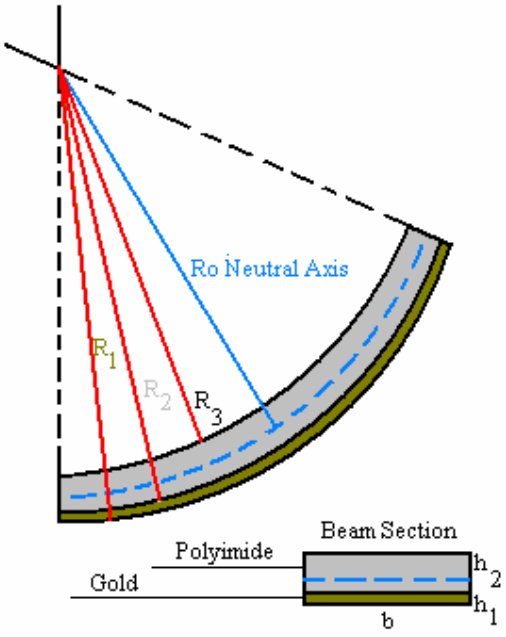

Fig._4.3._Geometric schematic of a bent beam.

By using Fig. 4.3, the curvature of a bent bimorph beam *(r)* and the vertical displacement of the free end *(Y)* under thermal strain without any slots could be obtained as bellow: *(L)* is the microcantilever length and *(D)* is the initial displacement of the free end of the beam.

$$\frac{1}{r}=\frac{1}{Ro}-\frac{1}{ro} \qquad \text{(Eq 4.5)}$$

$$Y=D-2\times r(Sin(\frac{L}{2r}))^2 \qquad \text{(Eq 4.6)}$$

$$ro=\frac{E1\times I}{M} \qquad \text{(Eq 4.7)}$$

Where *(Ro)*, *(I)* , *(E1)* and *(M)* are the beam bending neutral axis, section moment of inertia, Module of elasticity and bending moment respectively. They are as following:

$$I=b\times\left[\frac{h1^3}{12}+n\times\frac{h2^3}{12}+h1\times(Yo-\frac{R1+R2}{2})^2+n\times h2\times(\frac{R2+R3}{2})^2\right] \qquad \text{(Eq 4.8)}$$

$$M=\Delta T\times b\times\left[h1\times(h1/2-Yo)\times E1\times\alpha1+h2\times(h2/2+h1-Yo)\times E2\times\alpha2\right] \qquad \text{(Eq 4.9)}$$

$$Ro = \frac{\frac{R1+R2}{2}\times h1 + n\times\frac{R2+R3}{2}\times h2}{h1+n\times h2} \quad \text{(Eq 4.10)}$$

$$Yo = R1 - Ro \quad \text{(Eq 4.11)}$$

where *(Yo)* stands for the distance between the neutral axis and the bottom of the gold.

The results *(Y)* are shown in table 4.1. The displacements of the beam free end obtained by the analytical solution are close to the experiments but for optimization we need the stress and curvature details that could not be modeled analytically. For this purpose, finite element analysis has been done and explained later.

Temperature Load ΔT ℃	**Displacement of the free end by analytical solution in μm**	**Displacement measured in experiments in μm**
10	7	5
20	12.69	7.5
30	18.57	17.5
40	24.61	25
50	30.80	32
60	37.16	67.5

Table._4.1._Comparison between the displacement obtained by the analytical solution and the experimental results.

4.2. Finite Element Analysis

Several FEA models were constructed to evaluate the behaviour of a slotted beam, which is difficult to model analytically. It should be noted that in all the FE analysis, the microcantilever is fixed in one end and free in the other.

4.2.1. Transient Thermal Analysis (Metal-Polyimide)

Firstly, however, in order to understand the temperature propagation through the beam, a Thermal Transient Analysis of a plain (unslotted) flat polyimide – metal beam was carried out using the 3-D SOLID70 element from the ANSYS software suite. The program provides for up to eight nodes with a single degree of freedom, *viz.* temperature, at each node [14]. SOLID70 has a 3-D thermal conduction capability. The element has eight nodes with a single degree of freedom, temperature, at each node. The element is applicable to a 3-D, steady-state or transient thermal analysis [14]. Fig. 4.4 shows the geometry of SOLID70 element.

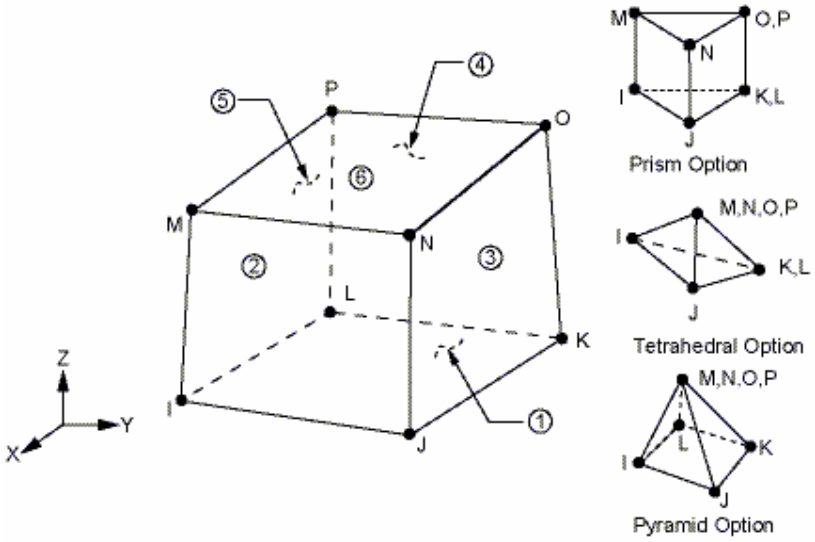

Fig._4.4._Geometric schematic of SOLID70 element.

The dimensions of the polyimide are 120µm x 450µm x 7µm and the aluminum is a uniform strip 0.2 µm thick and 5µm wide. The temperature profile response calculated vertically through the beam was obtained for a step increase in temperature of 100℃ at the top surface. The initial condition for all nodes was 20℃ (Figs. 4.5, 4.6).

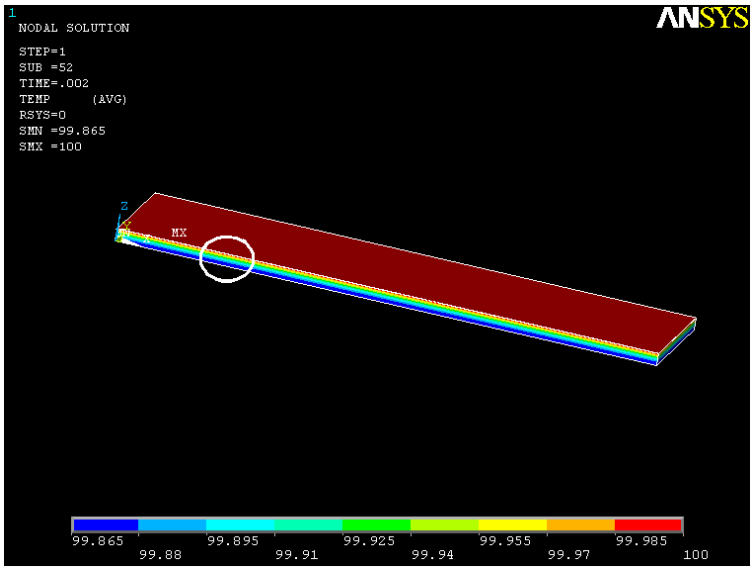

Fig._4.5._Aluminum Strip and Polyimide Transient Thermal analysis

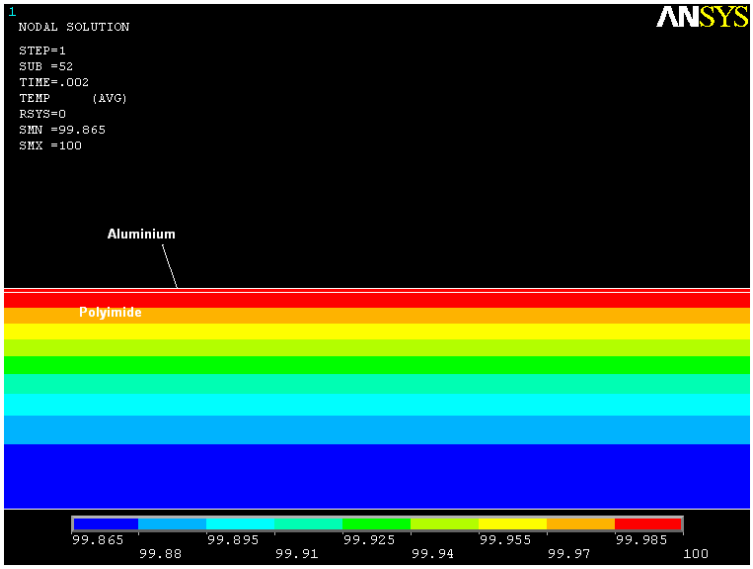

Fig._4.6._Zoomed Area of Figure 4.5

Fig. 4.7 shows how the temperature at the bottom of the polyimide beam, far away from the strip heater, varies with time; the steady state is reached in just 2µs. For the purposes of our

application, we can therefore assume that temperature in all nodes through the thickness of the microcantilever rises instantaneously to the load temperature.

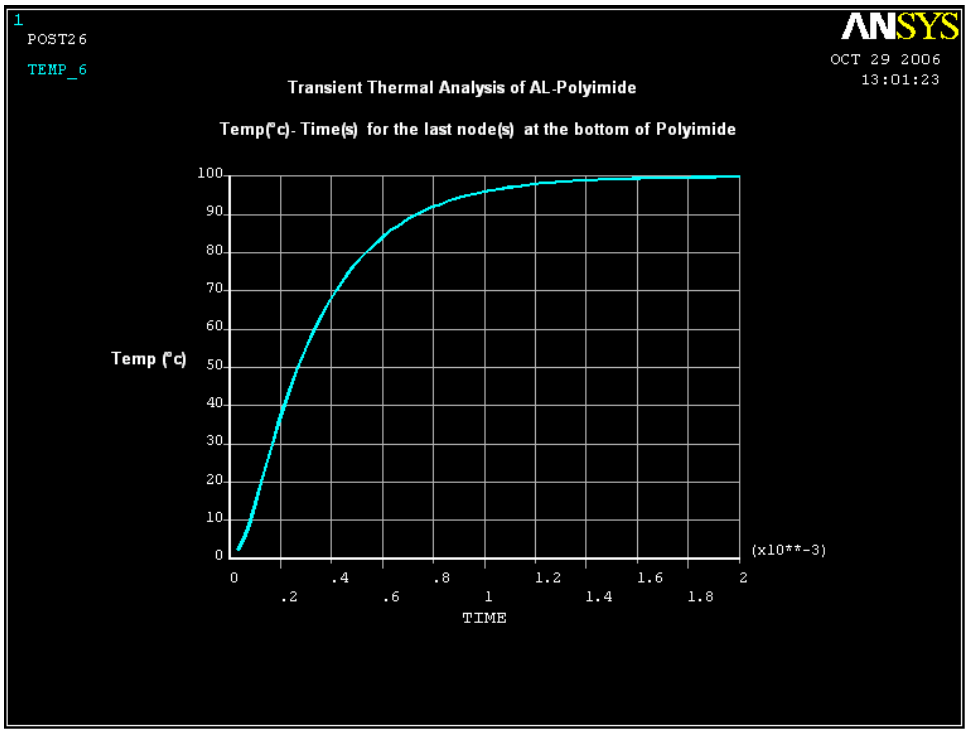

Fig._4.7._Temperature versus time on the bottom surface of the polyimide microcantilever.

As it can bee seen, and the curves are practically identical, these figures show that the Temperature propagation over time is 2 nano seconds for Aluminum and 2 micro seconds in Polyimide.

An important result from this analysis is that in the thermal-structural analysis, it is not necessary to consider the thermal-transient analysis. As the structure heated very fast so steady state in thermal analysis is enough means the temperature in all nodes are the same and are equal to the load temperature. This fact reduces the time when one uses numerical analysis.

The experimental results from [10] are shown in table 4.2. A maximum radius of curvature of 531μm, corresponding to a maximum deflection of 67.5μm, was achieved when the temperature rose to the maximum value of 100℃. Thi s corresponds to a maximum focal length of 265.5μm.

Temperatura [°C]	∆ T [℃]	Y [µm]	D [µm]	r [µm]	Focal length [µm]
40	0	250	0	355	177.5
50	10	245	5	364	182.5
60	20	242.5	7.5	370	185
70	30	232.5	17.5	388	194
80	40	225	25	411	205.5
90	50	218	32	427	213.5
100	60	182.5	67.5	531	265.5

Table._4.2._Experimental results showing the thermal response of the bimorph actuator [10].

Y is the total deflection of the beam. In practice, a flat bimorph microcantilever never occurs since the beam has an initial curvature due to stresses induced by the fabrication process. D is the temperature dependent additional displacement at the free end, from the 250µm base deflection at room temperature due to the intrinsic stresses.

4.2.2. Thermal Structural Analysis (Metal-Polyimide)

Attention was now turned to modeling the thermally driven micro-bimorph cantilever actuation of the slotted beam required for X-ray focusing applications. This made use of the SOLID 45 3-D element, which provides for eight nodes with three degrees of dimensional freedom at each node, *viz.* translations in the x, y, and z Cartesian directions [14] (Fig. 4.8).

In this study, both linear and large deformation non-linear analysis were employed and compared with the experimental results from [10]. The model beam consists of polyimide of thickness 7µm and gold of thickness1µm. The length of the beam is 450µm and its width is 120µm.

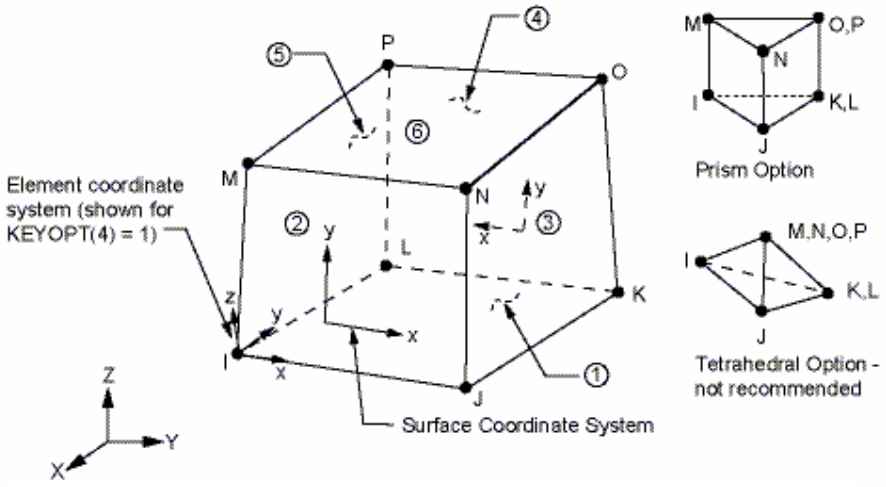

Fig._4.8._SOLID45 Geometry.

Another issue which should be defined is the linearity of analysis. Both types, the linear and non-linear analysis, are employed and compared with the experimental results (Fig. 4.9). Fig. 4.10 demonstrates the steady state thermal and nonlinear structural analysis of a flat beam consists of two materials (Polyimide and Gold).

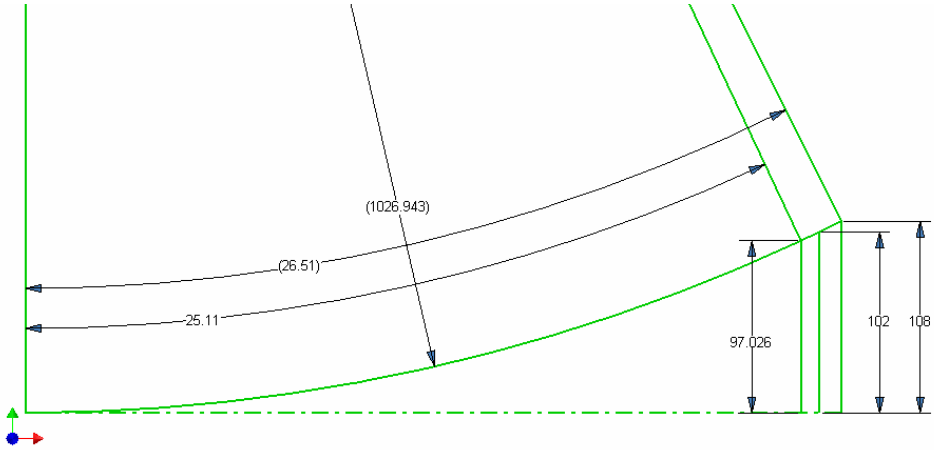

Fig._4.9._Comparison between the displacements of the free end of the beam obtained by several methods. 97,102 & 108µm are the Analytical, Linear & Nonlinear FEA

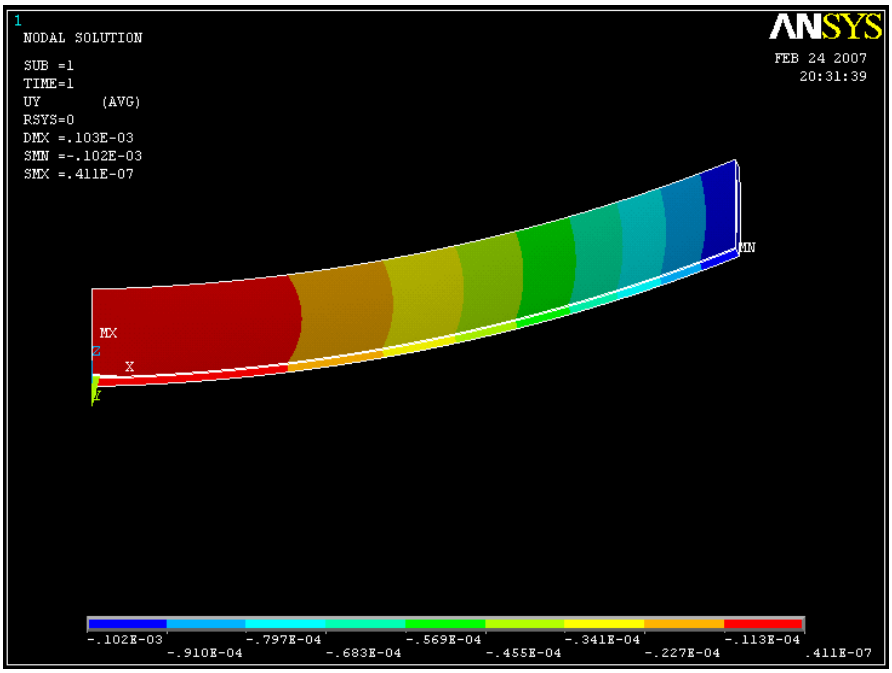

Fig._4.10._Thermal-NonLinear Structural analysis of a flat beam.

Displacement obtained from analytical solution which is given by equation 4.1 is 97µm while the value for linear and nonlinear analysis are 102µm and 108µm respectively, corresponding error values are 4% and 10% in displacement in ΔT=100℃.

The initial displacement of the free end of the micro slotted lens in the experimental results is 250µm [3, 4]. The displacement obtained from the analytical solution, linear and nonlinear FEA are 156µm, 163µm and 173µm in T=200℃, ΔT=160℃. As it is clear these results are far from the experiment.

4.2.3. Thermal-Structural Analysis of a Flat Slotted Beam

Analytical model can be used for a non-slotted beam and the results are very far from the experiments of a slotted beam. The results of the finite element analysis of the non-slotted beam are not proper approximations. Aiming at a better agreement with the experiments, we introduce now the slots into the mode. In this part for the first time, we consider the flat slotted beam.

In the simplified manufacturing process of the cantilever, the thermal bimorph cantilever was fabricated using Optical lithography from light sensitive polyimide (Dupont PI 2566) and sputter – coated gold in 200℃ and ΔT=160℃. The slots on the beam were fabricated at the end of manufacturing process and then the bent beam was achieved [10].

The slots on the microcantilever used in numerical analysis are the same as the real lens but firstly the flat slotted beam is considered.

To find out the initial displacement of the microcantilever which is 250µm in the experiments, one can see Fig. 4.11 illustrates the tip thermal-nonlinear structural finite element analysis. Table 4.3 summarized the initial displacement obtained by the experiments and both the linear and non linear finite element analysis. Fig. 4.12 shows the stress results obtained from the thermal-Nonlinear structural analysis using ANSYS.

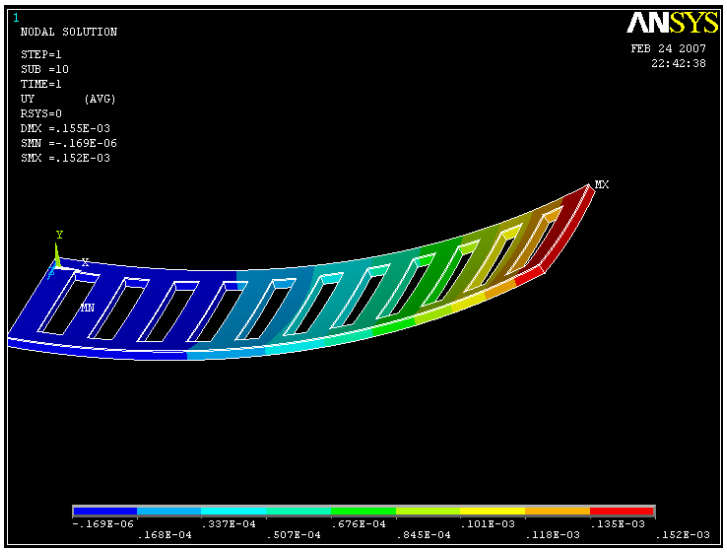

Fig._4.11._Displacement results obtained from Thermal-Non Linear Structural Analysis.

Fig._4.12._ Stress results obtained from Thermal-NonLinear Structural Analysis.

Initial Displacement using Linear FEA of a flat slotted beam in 200℃ in µm	Initial Displacement using nonlinear FEA of a flat slotted beam in 200℃ in µm	Initial Displacement obtained in the manufacturing process in µm
161	**156**	**250**

Table._4.3._Comparison between the displacements of the microlens obtained by the FEA & the experiment.

The important consequence of this analysis is that it is difficult to obtain the initial displacement using a flat slotted beam analysis, the reason could be that the manufacturing process modeling is more complex rather than only modeling of the modeling of thermal

coupling obtained by two dissimilar materials. So, one could consider the finite element analysis of the bent microcantilever which is explained in section 4.2.4.

Before going to the next section, there is an important question here, what is the curve of the bent beam? in order to know that how it approximate a circle we increased the temperature load on the flat beam finite element analysis by trial and error until the initial displacement of the flat slotted beam reach at 250 µm. Then by having this initial displacement one can obtain the curvature of the curved beam. Fig. 4.13 says that how the bent beam approximate a circle.

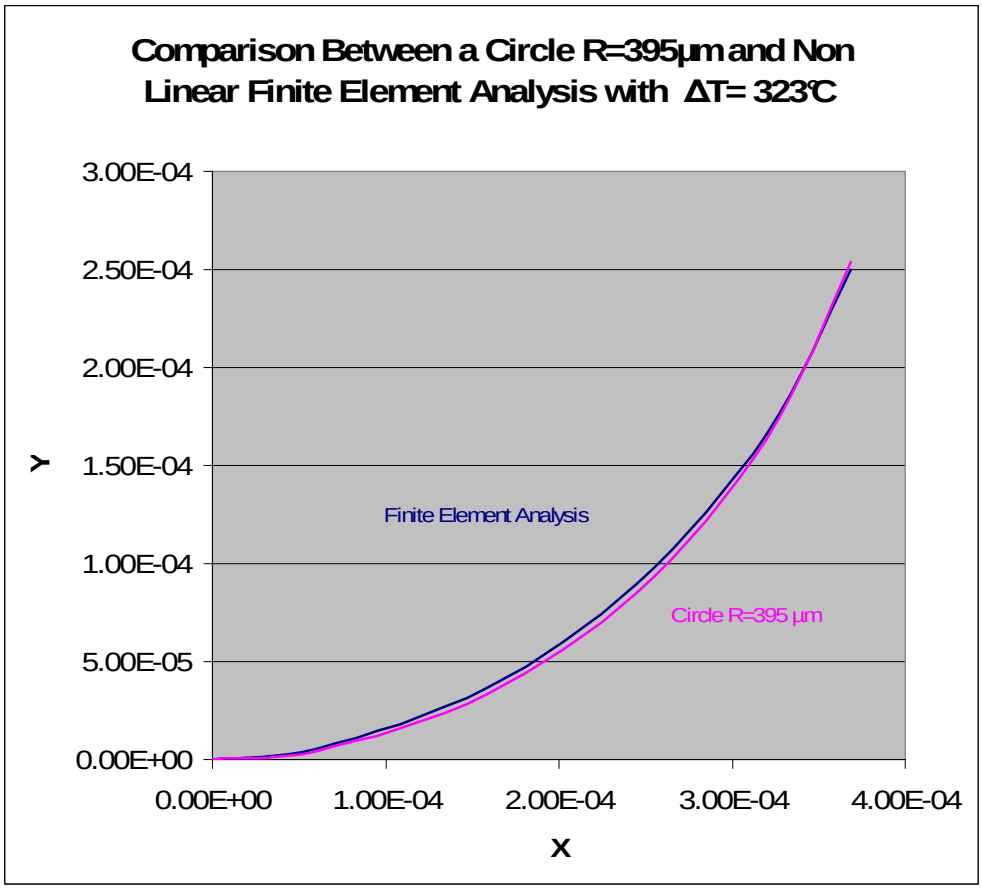

Fig._4.13._ How the bent beam approximates a circle.

As it is clear from Fig. 4.13, a circle with r = 395 µm is very close to the slotted beam which is bent through a temperature load of ΔT= 323℃ using finite element analysis. The significant note is that the maximum deviation between the circle and the curvature of the bent beam is less than 0.5%. These results leads us that the bent slotted lens can be modeled as a perfect arc of circle based on the focal length obtained in the experiments.

4.2.4. Thermal-Structural Analysis of a Bent Slotted Beam

The slotted beam was modeled, assuming it to be initially an arc of a circle, for ultimate comparison with the experimental results. Fig. 4.14 shows the tip displacement obtained from a Nonlinear structural and steady-state thermal analysis when T=80℃. The appearance of the linear model is similar and will not be shown here. Table 4.4 comprises the linear and nonlinear FEA of the T= 50℃, T= 60° C, T= 70℃, T= 80℃, T= 90℃ and T= 100℃.

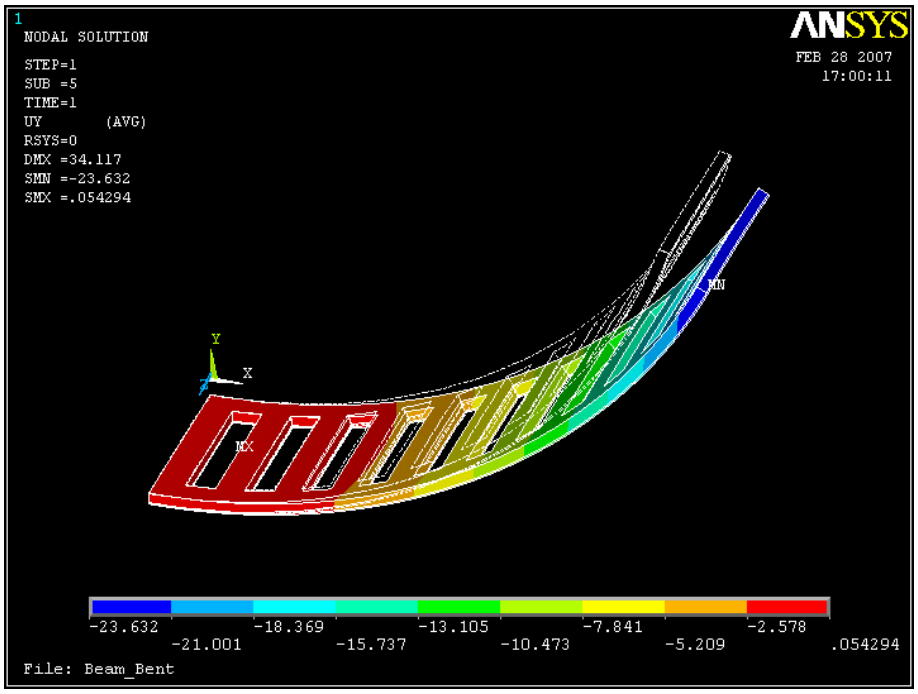

Fig._4.14._ Microcantilever form in T=80℃, showing end deflection. The skeleton shape is the initial form of the microcantilever.

Temperatura [°C]	ΔT [℃]	Displacement result using linear FEA in μm	Displacement result using nonlinear FEA in μm	Experimental results in μm
40	0	0	0	0
50	10	5.5	5.83	5
60	20	11	11	7.5
70	30	16.49	17.3	17.5
80	40	21.99	23.6	25
90	50	27	29.9	32
100	60	33	36.6	67.5

Table._4.4._Comparison between the displacements of the bent microlens obtained by the different FEA & experiments.

The curves obtained from the FEA models, compared with a perfect circle obtained from the experiments [3], for a range of temperatures are shown in Figs. 4.14 – 4.20

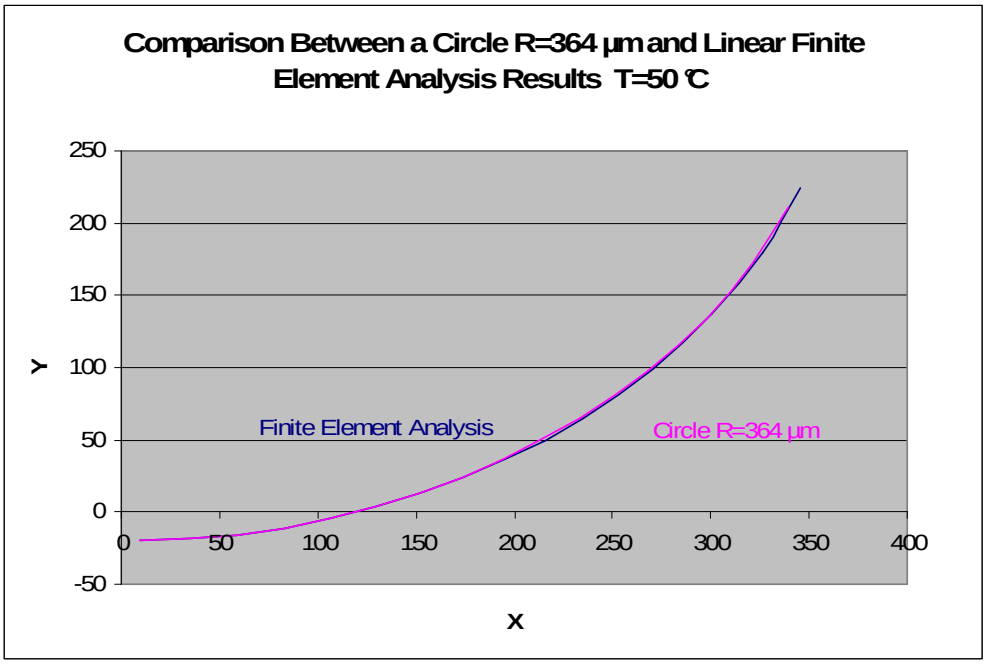

Fig._4.15._Comparison between experimental deflection and linear FEA results at T=50℃.

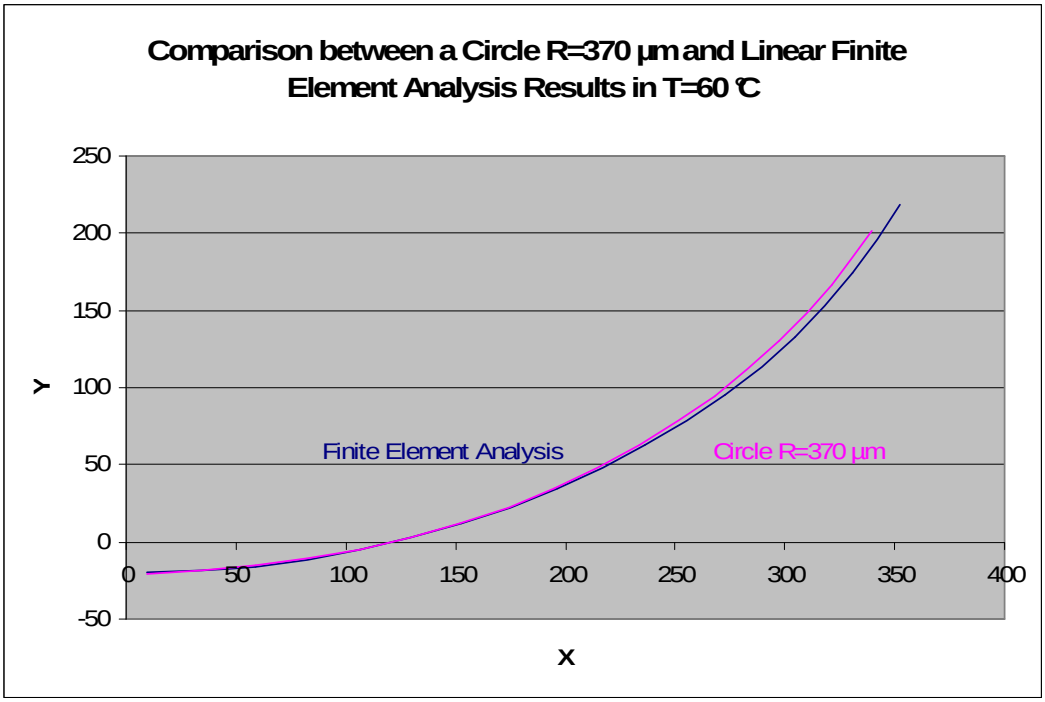

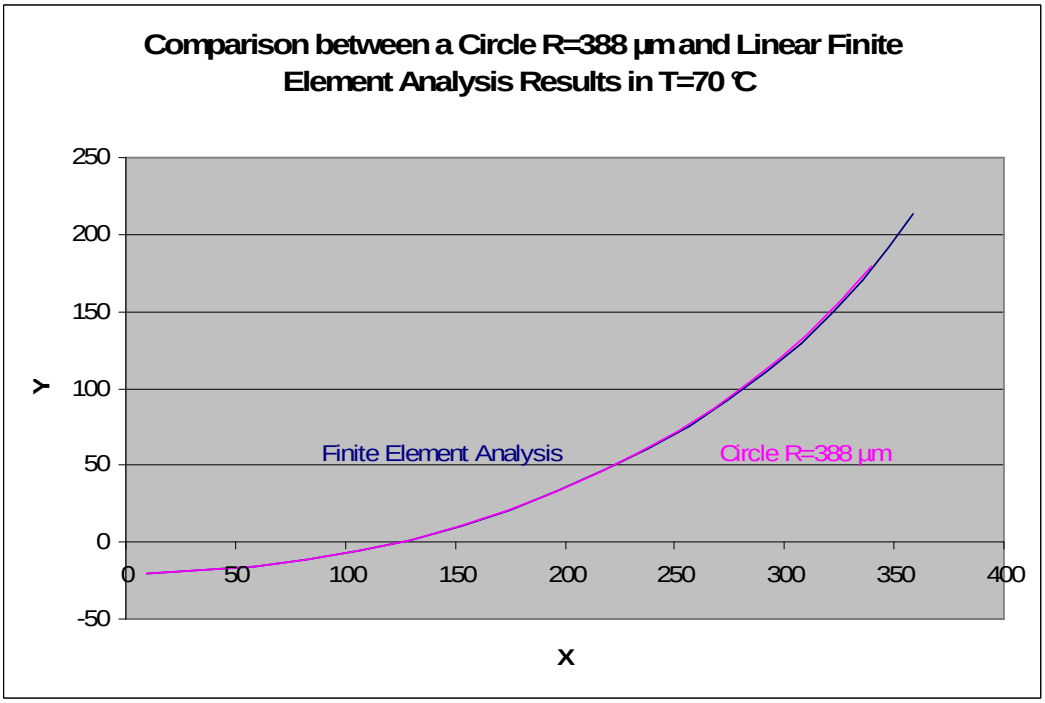

Fig._4.16, 4.17._Comparison between experimental deflection and linear FEA results at T=60℃, T=70℃.

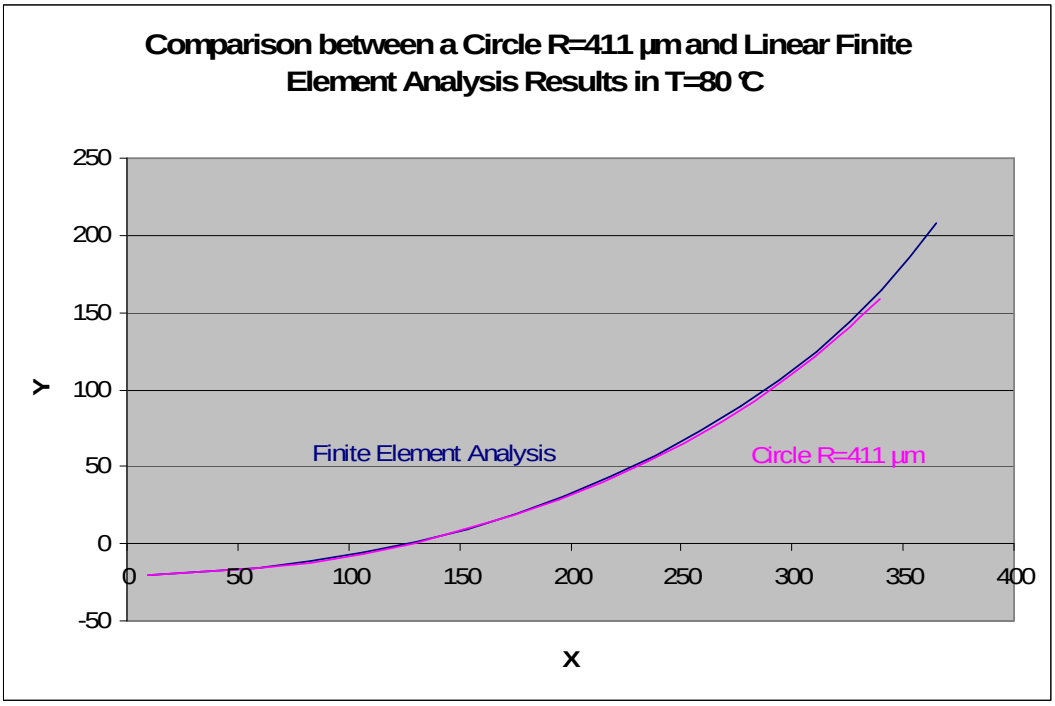

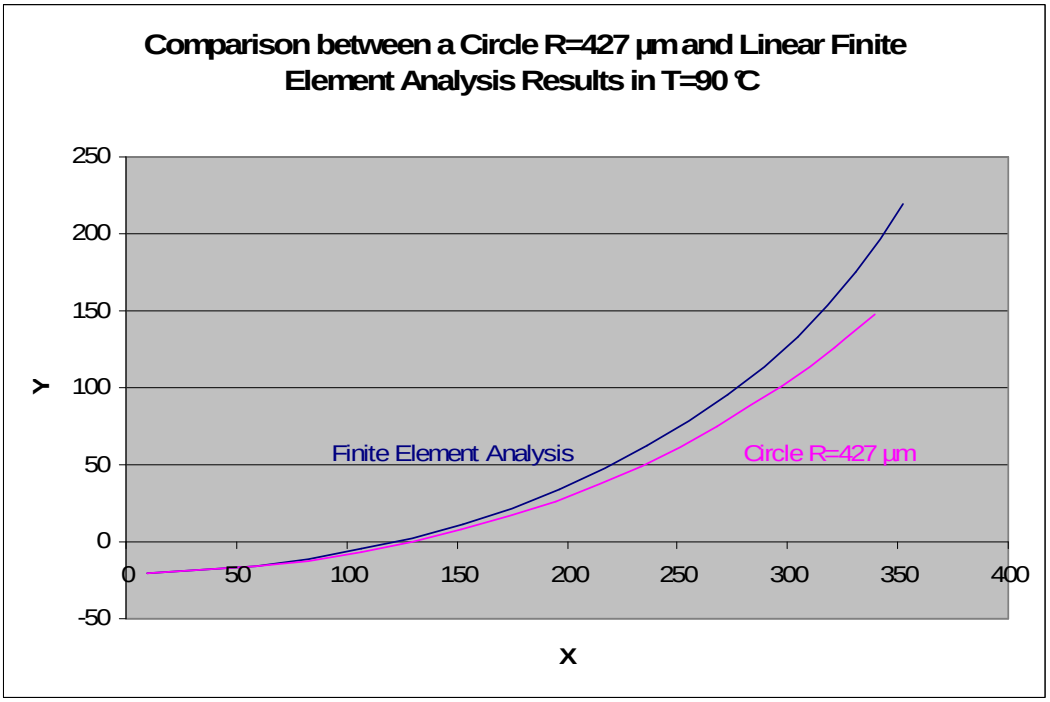

Fig._4.18, 4.19._Comparison between experimental deflection and linear FEA results at T=80℃, T=90℃.

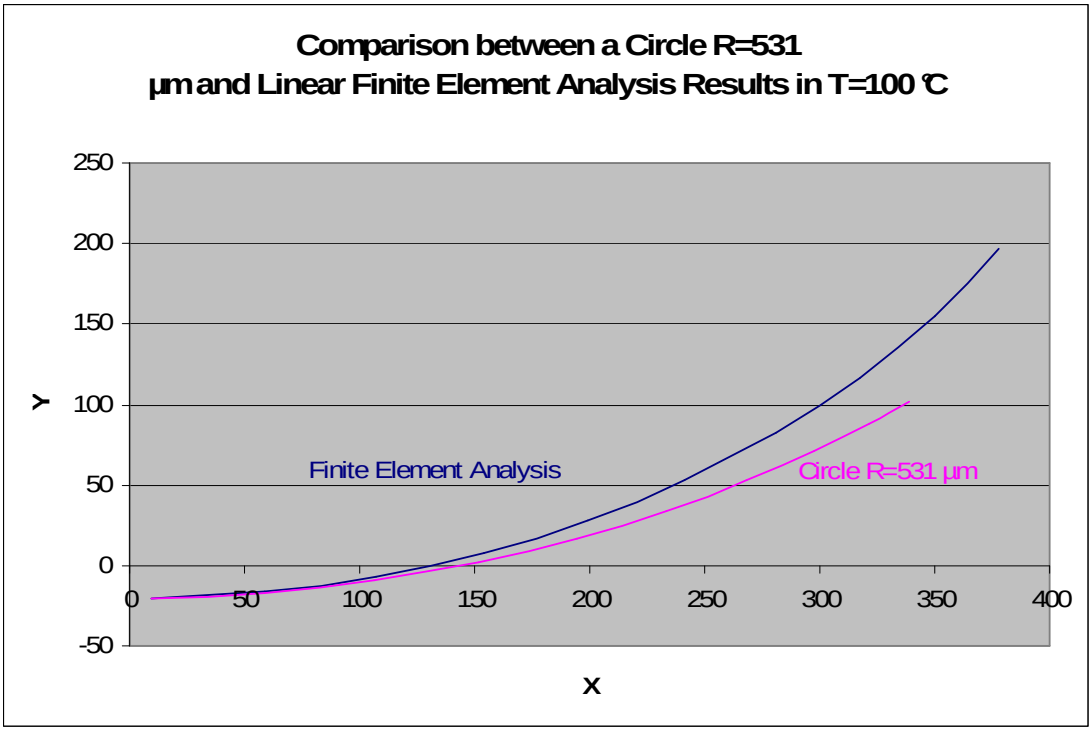

Fig._4.20._Comparison between experimental deflection and linear FEA results at T=100℃.

The curves obtained from the non linear FEA models, compared with a perfect circle obtained from the experiments [3], for a range of temperatures are shown in Figs. 4.21 – 4.26.

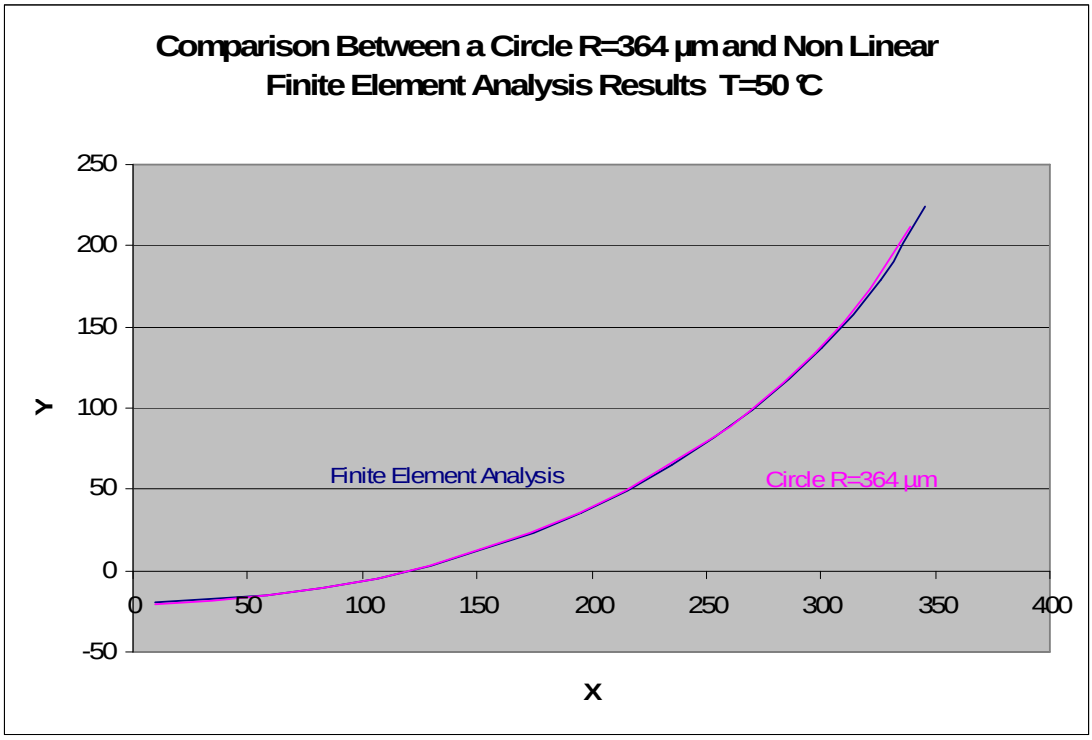

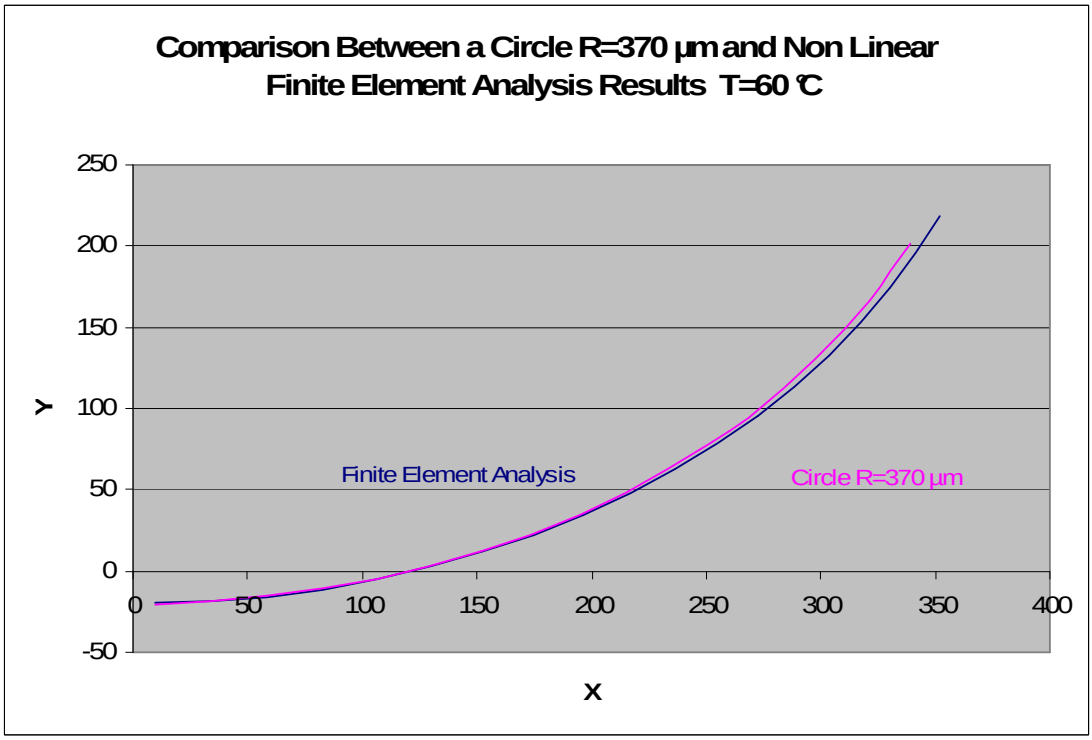

Fig._4.21,4.22._Comparison between experimental deflection and nonlinear FEA results at T=50℃,T=60℃.

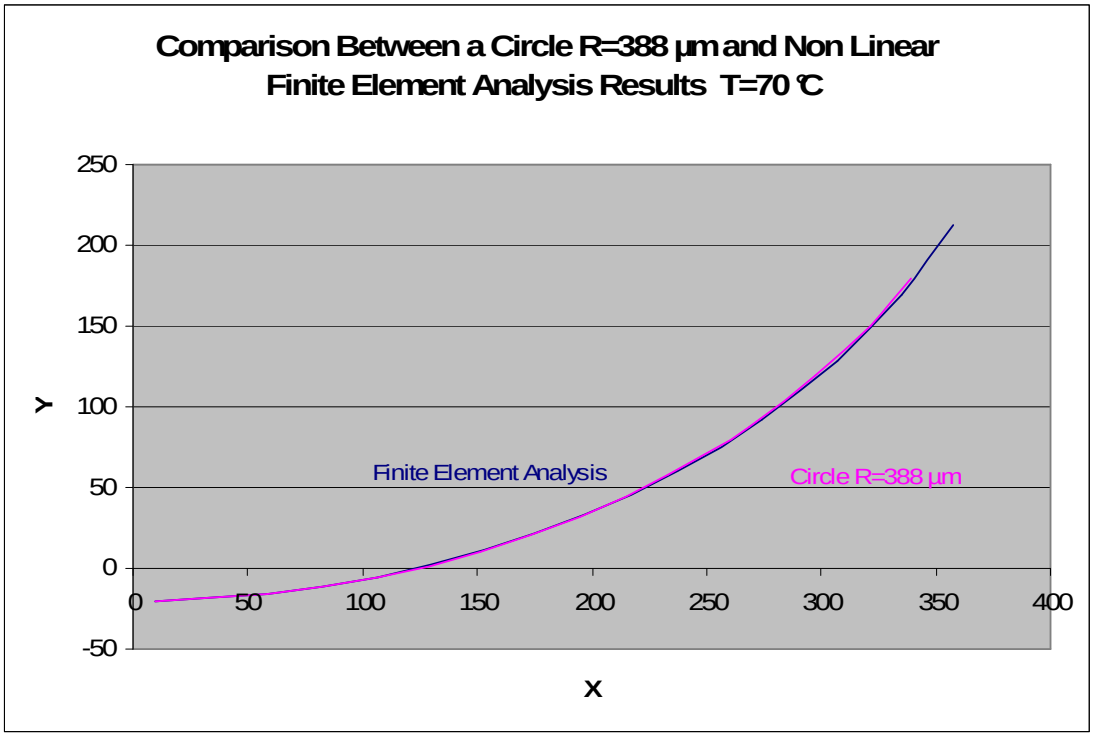

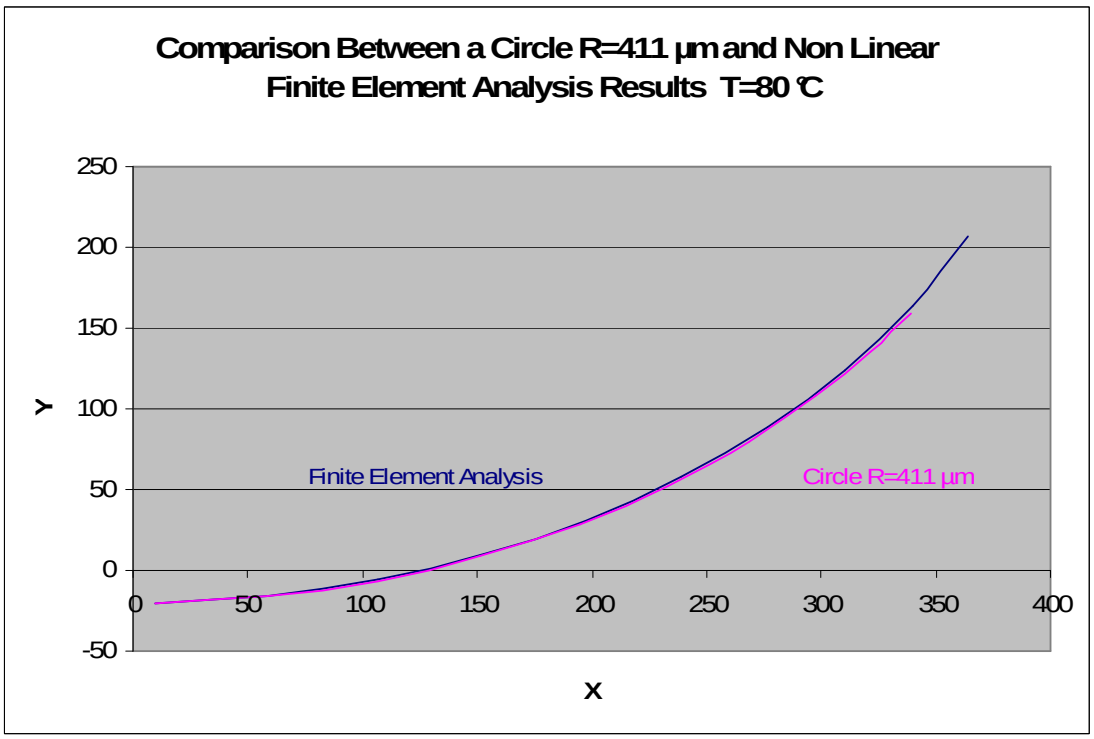

Fig._4.23,4.24._Comparison between experimental deflection and nonlinear FEA results at T=70℃,T=80℃.

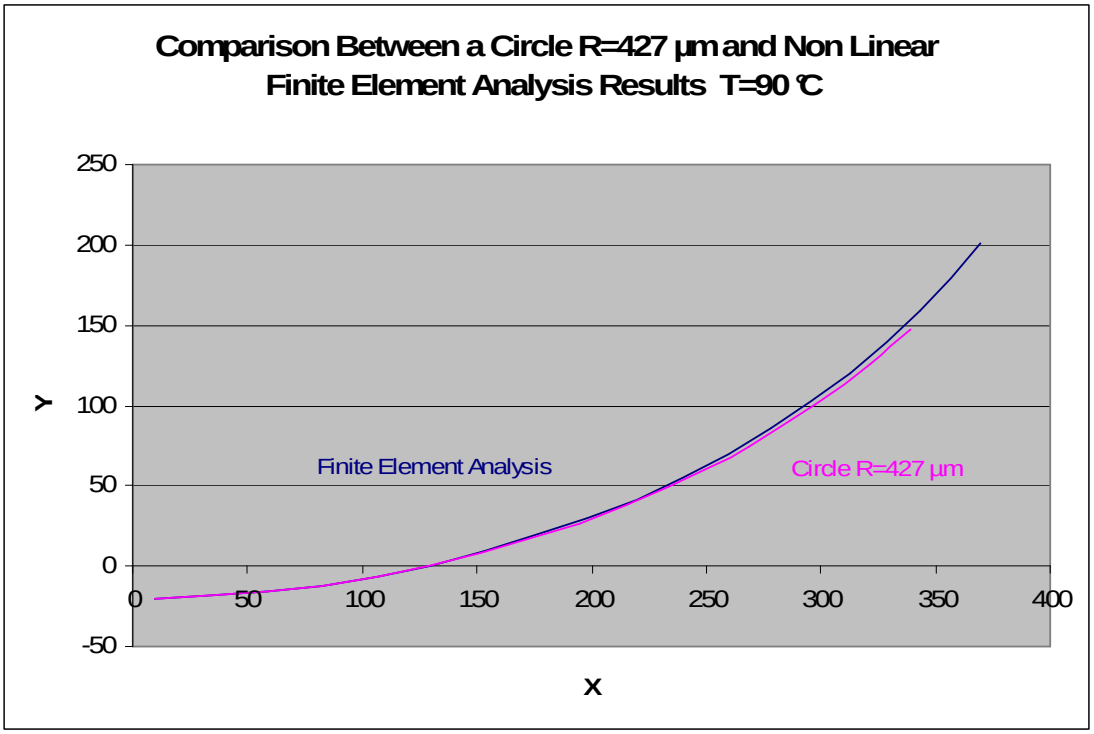

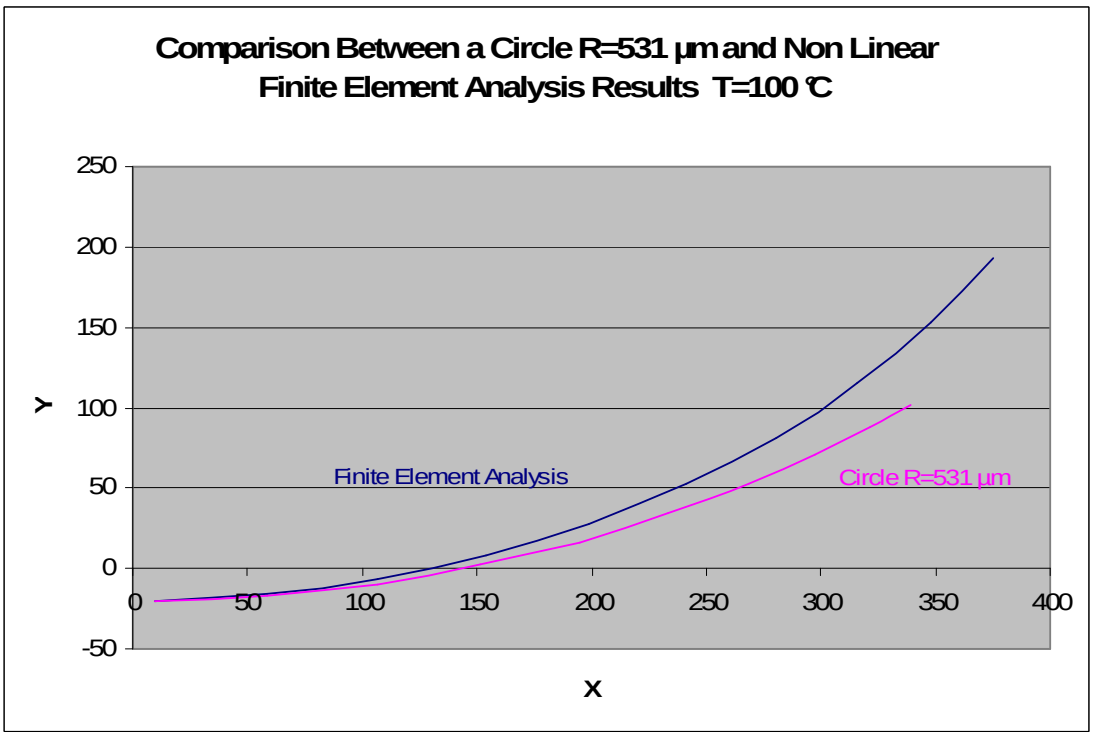

Fig._4.25,4.26._Comparison between experimental deflection and nonlinear FEA results at T=90℃,T=100℃.

Both sets of results – those based on a linear FEA and those using a non-linear model - show excellent agreement with experiment at temperatures up to 90℃. However, at 90℃ and above, the linear model diverges from experiment. Contrastingly, the non-linear model continues to show excellent agreement with experiment up to and including a temperature of 100℃. This model too shows strong divergence f rom theory at 100℃. This is consistent with the observations of Al-Aioubi *et al* [11], who report irreversible distortions above this temperature due to changes in the elastic properties of the polyimide.

5. Optimization

Optimization of the microlens from the standpoint of its mechanical properties is an important issue which can be resolved by FEA. The key question is: how does the stress in the microcantilever vary with the number of slots? The number of slots should be the maximum possible in order to maximize X-ray transmission, but this is naturally limited by the need to maintain structural integrity under thermal actuation. The modeled dimensions are 450µm length, 250µm initial displacement, thickness 8µm. In this optimization process the slot length is fixed. Only the number of slots and their width are varied. The proven non-linear FEA approach was used. The data from finite element analysis of slotted beams with 1, 3, 5, 7 and 11 slots are given in Fig. 5.1. The finite element analyses of the slotted beams are compared with a perfect circle. In this analysis the widths of slots are 20µm and the length 90µm. The result for the case of 5 slots is shown in Fig. 5.2.

Another assumption in this section is that, the distance between the slots is equal to the distance of the both end slots to the both free and fixed ends of the beam.

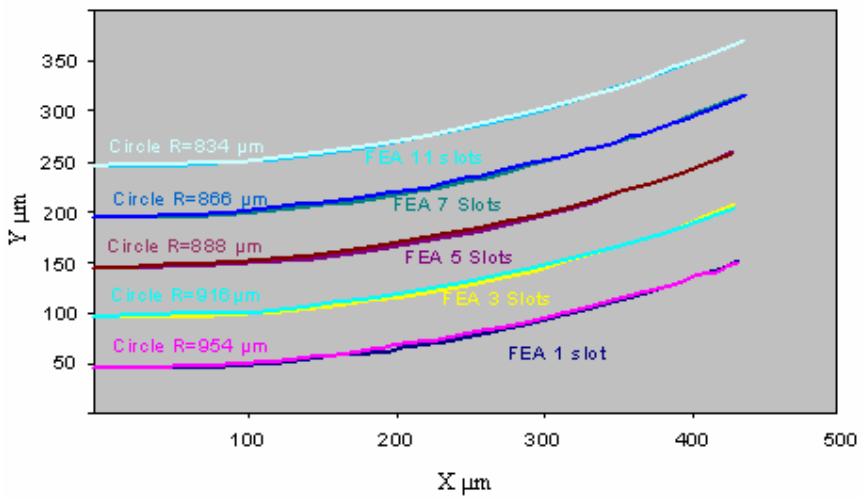

Fig._5.1._Curvature data obtained from Finite Element Analysis of slotted beams with 1,3,5,7 & 11 slots compared with perfect circle.

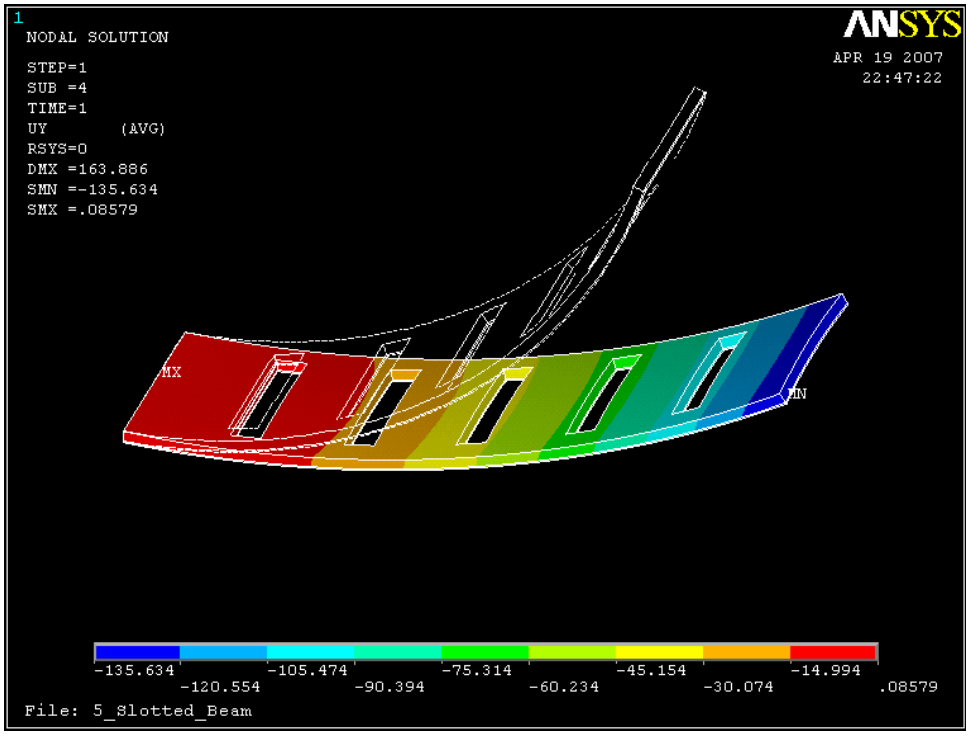

Fig._5.2._ Tip Non-linear FEA for a slotted microcantilever with 5 slots. The Skeleton shape is the initial form of the microcantilever.

This analysis has been done for several samples as below, all for the same temperature rise, ΔT=45℃.

- 1, 3, 5, 7, 11 slots, 20µm wide.

- 1, 3, 7, 13, 27 slots, 8µm wide.

- 1, 3, 7, 13, 27, 55 slots, 4 µm wide.

- 1, 3, 7, 13, 27, 55, 111 slots, 2µm wide.

The results, showing maximum and minimum stresses in the microlens (at the fixed and free ends respectively – refer to Fig. 5.2) as a function of the number of slots, are summarized in Figs. 5.3 – 5.10 in the next page.

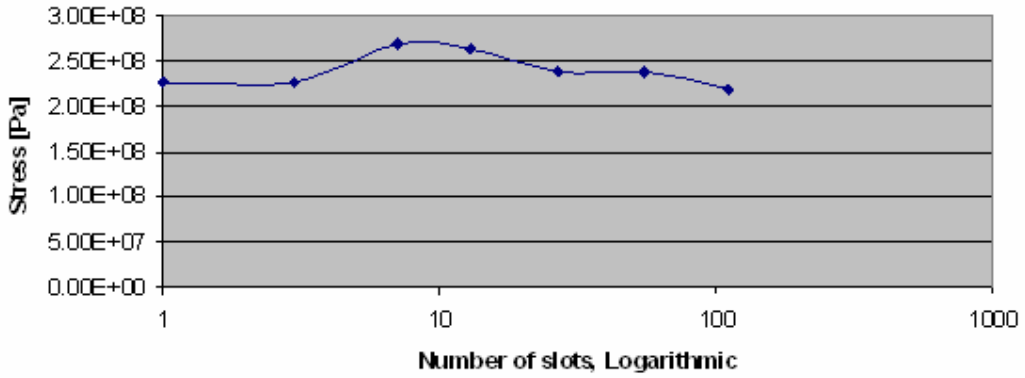

Fig._5.3._ Max Stress/No. of Slots, width of slots is 2µm and ΔT=45℃

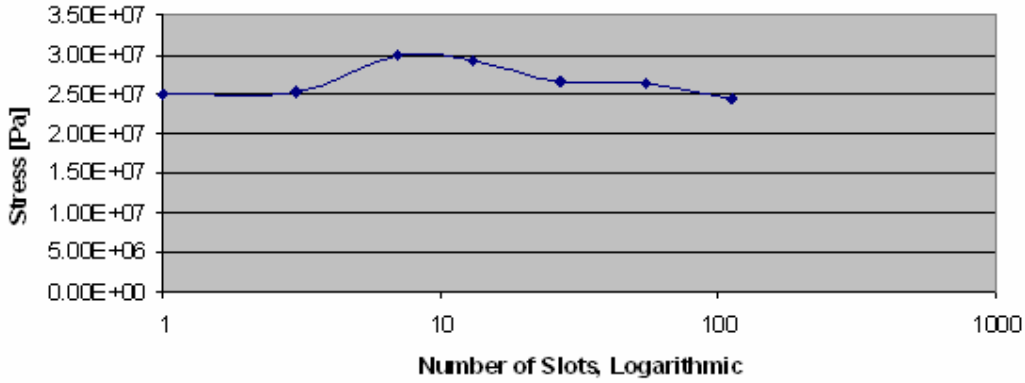

Fig._5.4._ Min Stress/No. of Slots, width of slots is 2µm and ΔT=45℃

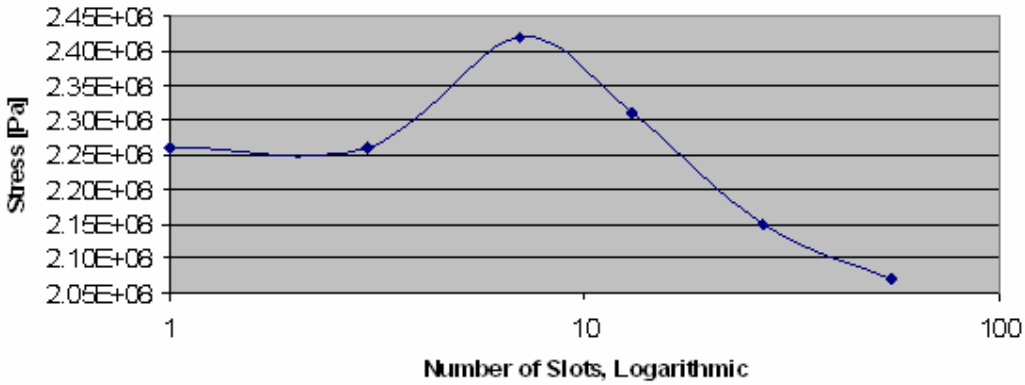

Fig._5.5._ Max Stress/No. of Slots, width of slots is 4µm and ΔT=45℃

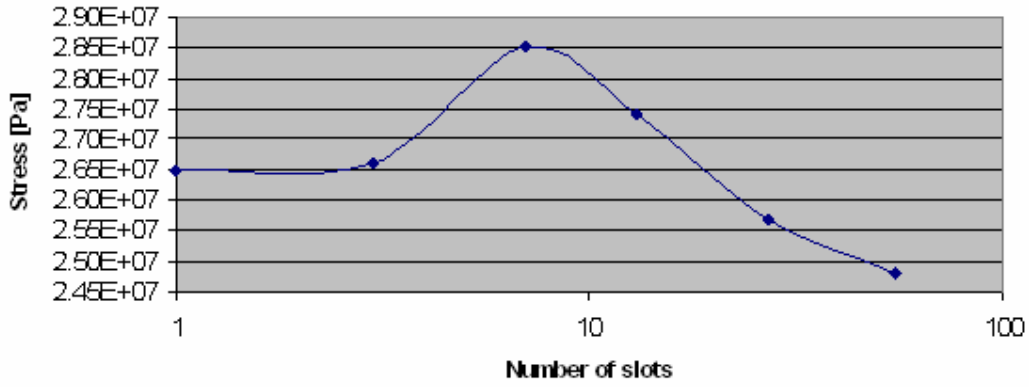

Fig._5.6._ Min Stress/No. of Slots, width of slots is 4µm and ΔT=45℃

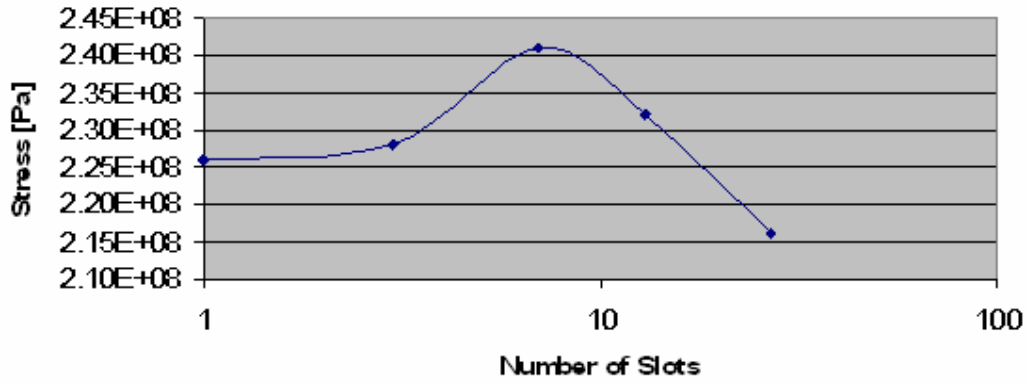

Fig._5.7._ Max Stress/No. of Slots, width of slots is 8µm and ΔT=45℃

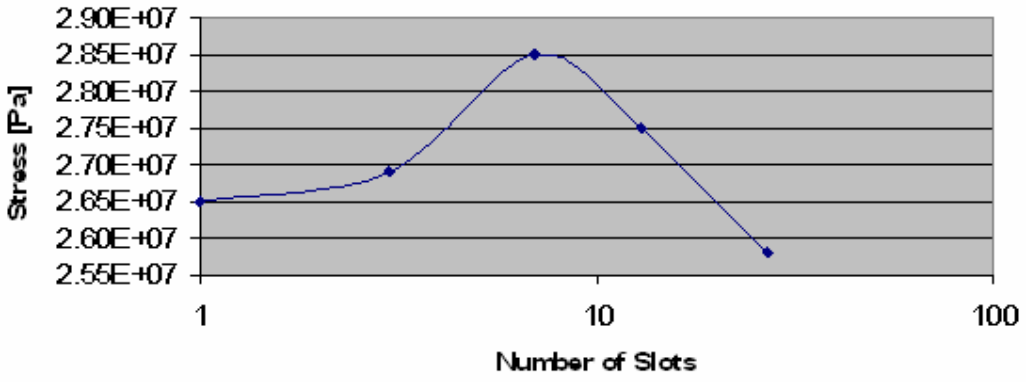

Fig._5.8._ Min Stress/No. of Slots, width of slots is 8µm and ΔT=45℃

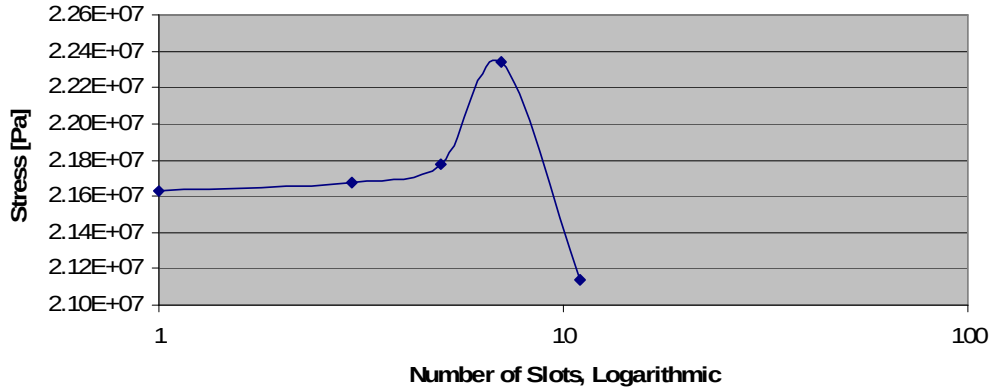

Fig._5.9._ Max Stress/No. of Slots, width of slots is 20μm and ΔT=45℃

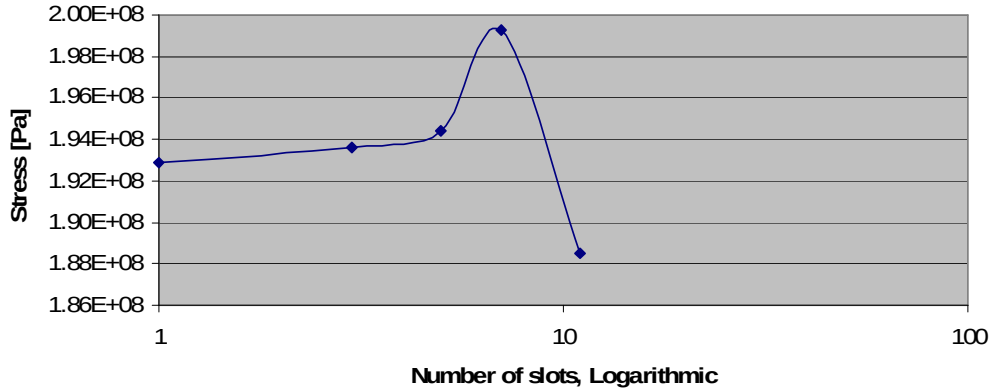

Fig._5.10._ Min Stress/No. of Slots, width of slots is 20μm and ΔT=45℃

Both minimum and maximum stresses increased with the number of slots. This increase peaks at roughly the same point for all cases (between 7 and 13 slots) after which the stress decreases. The stresses are not strongly dependent on the width of slots, depending rather on their number. The variation of tip deflection with slots was also determined, for selected slots widths and temperatures, with the results shown in Figs. 5.11 to 5.13.

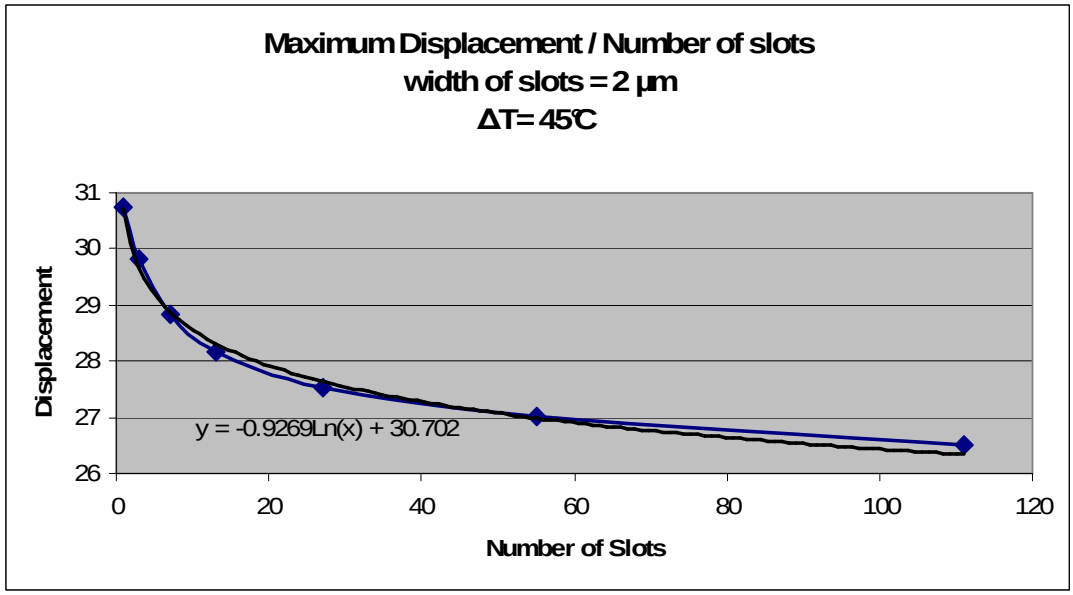

Fig._5.11._ Tip displacement (µm) /Number of slots; width of slots is 2µm, ΔT=45°C.

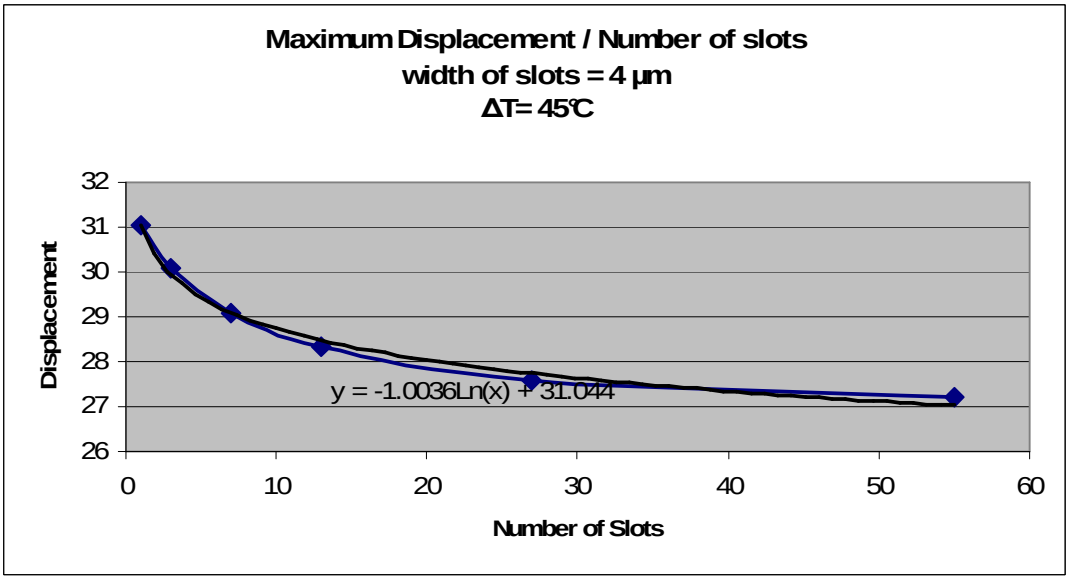

Fig._5.12._Tip displacement (µm) /Number of slots; width of slots is 4µm, ΔT=45°C.

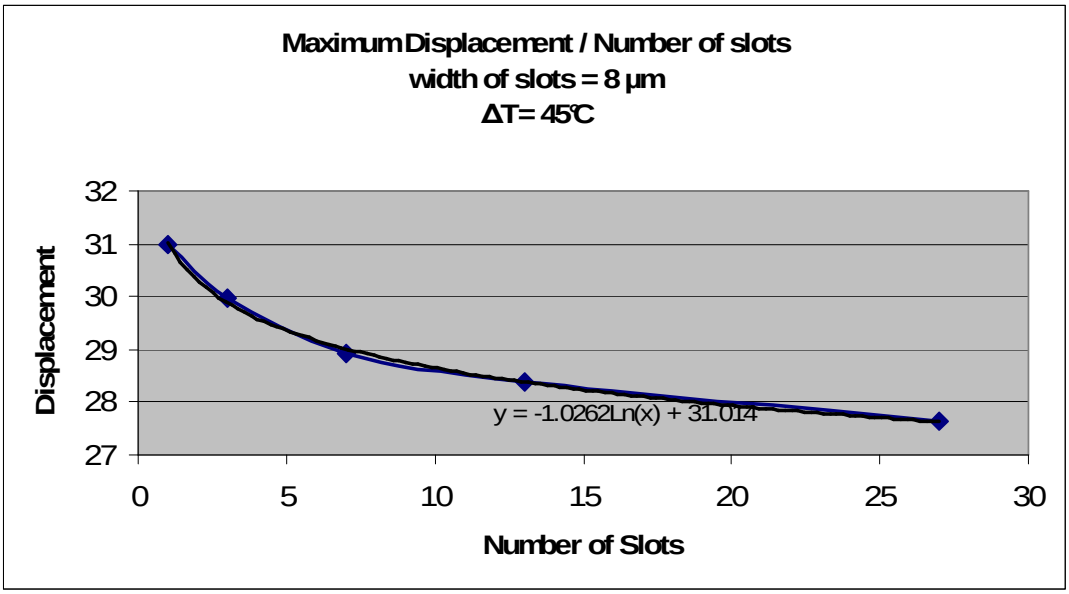

Fig._5.13._Tip displacement (µm) /Number of slots; width of slots is 8µm, ΔT=45℃.

For low temperature rise of ΔT=45℃, the tip deflection response has an approxim ately similar exponential dependence, given by equations 5.1 to 5.4 below. The displacement does not depend on the width of slots.

Slot width 2µm: $y = -0.9269 \ln(x) + 30.702$ (Eq. 5.1)

Slot width 4µm: $y = -1.0036 \ln(x) + 31.044$ (Eq. 5.2)

Slot width 8µm: $y = -1.0262 \ln(x) + 31.014$ (Eq. 5.3)

Slot width 20µm: $y = -1.2166 \ln(x) + 36.761$ (Eq. 5.4)

As mentioned earlier there is a clear number of slots for each slot width at which the internal stress in the structure is maximized. Also the curvature, which is arguably the most important parameter in the optimization of the micolens is closer to a perfect circle as the number of slots increases. The predicted displacement does not depend on the number of slots, but, for beams with narrower slots, the mapped function and the FEA data are closer to each other. Since microfabrication using optical lithography restricts the readily achievable slot width to approximately 2µm and bearing in mind the foregoing, an optimized

structure for our 450µm long microcantilever would have 111 slots of width 2µm. The results of non-linear FEA analysis for such a structure are shown in Fig. 5.14.

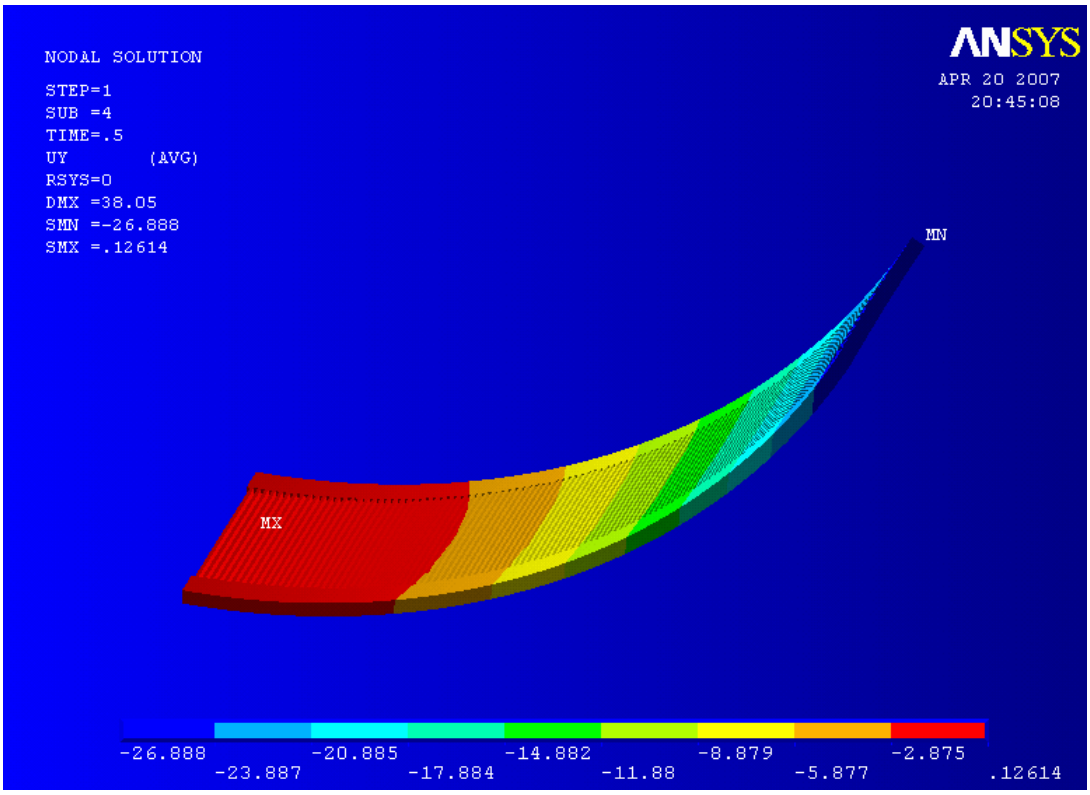

Fig._5.14._FEA analysis (non-linear) for an optimized microlens, of length 450µm ; 111 slots, 2µm wide.

Final Results

- The study of the non slotted flat beam analytically and numerically showed that the displacement obtained from the FEA analysis in this case is 3%-5% more than the analytical solution. The FEA results in displacement are closer to the experiments but however they are 40% farther than the reality.

- The Transient thermal FEA of the Aluminum strip and polyimide described that due to the fast propagation of the temperature through the beam, it is not necessary to consider the transient thermal analysis in the next steps. It reduces the time of the FEA analysis. The structural analysis in all of the FEA is steady state as the response of the lens is not very fast [10].

- As it was mentioned before, the linear and non linear structural analysis of the flat slotted beam has been applied and this analysis represented that the results of the displacement is still far from the experiments. In fact the results of the non-slotted beam are closer to the experiments rather than the slotted one.

- Last but not least, the bent beam was considered, in the FE analyses of the bent beam; this fact became clear that the Nonlinear FE results are better rather than the linear structural analysis and the analysis can describe the behavior of the lens properly. The curvature of the beam is an utmost important issue which affects the focal point quality. The FEA of the micro lens showed that the micro lens remains as an arc of a circle after the temperature load.

- Finally, in the optimization section, one can understand that by increasing the number of slots the curvature follow an arc of a circle better. Also, there is special number of slots in which the maximum and minimum stress happens on the beam regardless of the width and number of slots. Actually, by increasing the number of the slots, the more material is removed from the structure which means that the stiffness and the thermal coupling decrease but the reducing of the thermal coupling is more effective and this is why the displacement of the free end of the slotted beam declines by increasing the number of slots, however, this effect is small enough to say that the beam free-end point displacement is not a function of the number of slots and their width. Then based on these results, a micro beam with 111 slots with the width of 2µm was suggested as an optimized imaging lens which is the maximum possible number of the slots on the beam regarding the manufacturing criteria.

Conclusion

A series of simulations using FEA analysis has shown the dependence of tip deflection, form and internal stresses on structure and temperature for microcantilever bimorph structures as designed for an X-ray focusing MOEMS (1-D MOXI). The critical importance of the number of slots in obtaining the spherical form necessary for aberration free spot formation has been shown. The superiority of non-linear FEA compared with linear FEA has been revealed by the study, but a simple analytical model is surprisingly good. An optimized structure containing 111 slots 2µm wide is shown to give a thermally actuated form very close to a perfect circle, as required for the 1-D MOXI MOEMS device.

References

[1] K. Atkinson, *"Methods of efficiently focusing $Ti_{K\alpha}$ X-Ray in low-brightness limited-Geometry systems"* MRes Thesis,2002, King's College London.

[2] C Mothersill and C Seymour, *"Low-dose radiation effects: Experimental hematology and the changing paradigm"*, International Society for Experimental Hematology, (2003) June 31 (6) 437–445, Published by Elsevier Inc.

[3] M Y Al Aioubi, P D Prewett, S E Huq, V Djakov and A.G. Michette, *"Micro-OptoElectro-Mechanical System for X-Ray Focusing"* Proc MNE06 Barcelona, for publication Microelectron Eng (2007)

[4] M Y Al Aioubi, P D Prewett, S E Huq, V Djakov and A.G. Michette, *"A Novel MOEMS based adaptive optics for X-ray focusing"* Microelectronic Engineering Volume 83 (2006), pp 1321-1325.

[5] A G Michette, *"Optical system for soft X rays",* 1986, Plenum Press, New York.

[6] ICE.Turcu and J BDance, *"X-rays from laser plasmas: generation and application*", 1999 John Wiley &Sons Ltd, England.

[7] P D Prewett and A G Michette, *"MOXI: A novel micro-fabricated zoom lens for x-ray imaging"*, Proc SPIE 4145, 2001.

[8] P D Prewett and A G Michette, *"UK Patent Application No9927631.3"*, November 1999

[9] P. Kirkpatrick and A. V. Baez, *"Formation of optical images by x-rays"* J. Opt. Soc. Am. 38 (1948) 766

[10] J Thaysen, A Yalçinkaya, P Vettiger and A. Menon, *"Polymer-based stress sensor with integrated readout"*, J. Phys. D: Appl. Phys. Vol. 35 (2002), pp 2698–2703.

[11] M Y Al Aioubi, V Djakov, S E Huq and P D Prewett, *"Deflection and load characterisation of bimorph actuators for bioMEMS and other applications"*, Microelectronic Engineering 73-74, 2004, 898-903.

[12] G Lammel, S Schweizer and P Renaud, *"Optical Microscanners and Microspectrometers Using Thermal bimorph Actuators"*, Kluwer Academic Publishers, Dordrecht (2002).

[13] E. J. Hearn, *"An Introduction to the Mechanics of Elastics and Plastic Deformation of Solids and Structural Materials",* Third Edition, 62-92, Elsevier Publication (1997).

[14] *ANSYS Release 9 Documentation*, SOLID70 and SOLID45 elements descriptions.

Complementary References

Ferdinand P. Beer,Jr., E. Russell Johnston,John T. DeWolf, *"Mechanics of Materials"* Third Edition, Mc Grow Hill Publication, (2002).

Michael Lai, David Rubin, Erhard Kremple, *"An Introduction to Continuum Mechanics"*, Third Edition, Elsevier, (1996).

http://www.mece.ualberta.ca/tutorials/ansys/

Appendix

Material properties used in ANSYS

MatWeb Data Sheet

Overview - Polyimide

KeyWords:
Plastics, Polymers
SubCat: Polyimide, Thermoplastic, Polymer

Properties	Value	Min	Max
Physical			
Density, g/cc	--	1.34	1.43
Water Absorption, %	--	0.24	0.4
Moisture Absorption at Equilibrium, %	--	1.2	1.3
Mechanical			
Hardness, Rockwell E	--	50	99
Hardness, Rockwell M	110	--	--
Tensile Strength, Ultimate, MPa	--	72.4	120
Tensile Strength, Yield, MPa	120	--	--
Elongation at Break, %	--	4	10
Tensile Modulus, GPa	--	1.3	4
Flexural Modulus, GPa	--	2.48	4.1
Flexural Yield Strength, MPa	--	82.7	200
Compressive Yield Strength, MPa	--	112	200
Compressive Modulus, GPa	--	2.41	3.1
Poissons Ratio	0.41	--	--
Fatigue Strength, MPa	44.8	--	--
Shear Strength, MPa	89.6	--	--
Izod Impact, Notched, J/cm	--	0.4	0.75
Izod Impact, Unnotched, J/cm	7.5	--	--
Coefficient of Friction	0.29	--	--
K Factor (Wear Factor)	50	--	--
Limiting Pressure Velocity, MPa-m/sec	0.35	--	--
Electrical			
Dielectric Constant	--	3.4	3.55
Dielectric Constant, Low Frequency	--	3.4	3.62
Dielectric Strength, kV/mm	--	22	27.6
Dissipation Factor	--	0	0.01
Dissipation Factor, Low Frequency	--	0	0.01

	Value	Min	Max
Thermal			
CTE, linear 20℃, µm/m-℃	--	45	90
CTE, linear 100℃, µm/m-℃	--	50	54
Specific Heat Capacity, J/g-℃	--	1.13	1.2
Thermal Conductivity, W/m-K	--	0.1	0.35
Maximum Service Temperature, Air, ℃	--	304	360
Deflection Temperature at 1.8 MPa (264 psi), ℃	--	280	360
Glass Temperature, ℃	--	323	340
Flammability, UL94	V-0	--	--
Oxygen Index, %	53	--	--
Processing			
Processing Temperature, ℃	320	--	--

Vendors
Matweb.com

Gold Properties

Physical	
Density, g/cc	19.32
Mechanical	
Hardness, Vickers	25
Modulus of Elasticity, GPa	77.2
Shear Modulus, GPa	27.2
Poisson Ratio	0.42
Thermal	
Heat of Fusion, J/g	66
CTE, linear 20℃, µm/m-℃	14.4
CTE, linear 250℃, µm/m-℃	14.6
CTE, linear 500℃, µm/m-℃	15.2
Specific Heat Capacity, J/g-℃	0.1323
Thermal Conductivity, W/m-K	301

MatWeb Data Sheet

Aluminum, Al

SubCat: Aluminum Alloy, Pure Element, Nonferrous Metal, Metal

Material Notes:

This listing is for pure aluminum.

Component	Value	Min	Max
Aluminum, Al	100		

Properties	**Value**	**Min**	**Max**
Physical			
Density, g/cc	2.6989	--	--
Mechanical	**Value**	**Min**	**Max**
Hardness, Vickers	15	--	--
Modulus of Elasticity, GPa	68	--	--
Shear Modulus, GPa	25	--	--
Electrical			
Electrical Resistivity, ohm-cm	2.70E-06	--	--
Magnetic Susceptibility	6.00E-07	--	--
Critical Magnetic Field Strength, Oersted	--	101.9	107.9
Critical Superconducting Temperature, K	--	1.73	1.77
Thermal			
Heat of Fusion, J/g	386.9	--	--
CTE, linear 20℃, µm/m-℃	24	--	--
CTE, linear 250℃, µm/m-℃	25.5	--	--
CTE, linear 500℃, µm/m-℃	27.4	--	--
Specific Heat Capacity, J/g-℃	0.9	--	--
Thermal Conductivity, W/m-K	210	--	--
Melting Point, ℃	660.37	--	--
Optical			
Emissivity (0-1)	--	0.2	0.3
Emissivity (0-1)	0.05	--	--
Reflection Coefficient, Visible (0-1)	0.9	--	--

Ansys Nonlinear solution Methods.

ANSYS employs the "Newton-Raphson" approach to solve nonlinear problems. In this approach, the load is subdivided into a series of load increments. The load increments can be applied over several load steps. The Figure illustrates the use of Newton-Raphson equilibrium iterations in a single DOF nonlinear analysis.

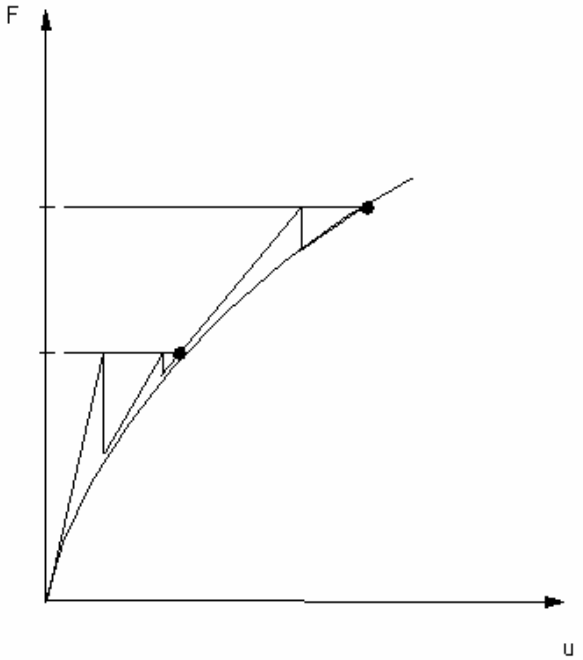

Full Newton-Raphson iterative solution (2 load increments)

Before each solution, the Newton-Raphson method evaluates the out-of-balance load vector, which is the difference between the restoring forces (the loads corresponding to the element stresses) and the applied loads. The program then performs a linear solution, using the out-of-balance loads, and checks for convergence. If convergence criteria are not satisfied, the out-of-balance load vector is reevaluated, the stiffness matrix is updated, and a new solution is obtained. This iterative procedure continues until the problem converges.

number of convergence-enhancement and recovery features, such as line search, automatic load stepping, and bisection, can be activated to help the problem to converge. If convergence cannot be achieved, then the program attempts to solve with a smaller load increment.

In some nonlinear static analyses, if you use the Newton-Raphson method alone, the tangent stiffness matrix may become singular (or non-unique), causing severe convergence

difficulties. Such occurrences include nonlinear buckling analyses in which the structure either collapses completely or "snaps through" to another stable configuration. For such situations, you can activate an alternative iteration scheme, the *arc-length method*, to help avoid bifurcation points and track unloading.

The arc-length method causes the Newton-Raphson equilibrium iterations to converge along an *arc*, thereby often preventing divergence, even when the slope of the load vs. deflection curve becomes zero or negative. This iteration method is represented schematically in the next figures.